

Formation and Evolution of Secondary Organic Aerosol Derived from Urban Lifestyle Sources: Vehicle Exhaust and Cooking Emission

Zirui Zhang^{§,1}, Wenfei Zhu^{§,1}, Min Hu^{*,1,2,5}, Kefan Liu¹, Hui Wang¹, Rongzhi Tang¹, Ruizhe Shen¹, Ying Yu¹, Rui Tan¹, Kai Song¹, Yuanju Li¹, Wenbin Zhang³, Zhou Zhang³, Hongming Xu³, Shijin Shuai³, Shuangde Li⁴, Yunfa Chen⁴, Jiayun Li⁶, Yuesi Wang⁶, Song Guo¹

¹State Key Joint Laboratory of Environmental Simulation and Pollution Control, International Joint Laboratory for Regional Pollution Control, Ministry of Education (IJRC), College of Environmental Sciences and Engineering, Peking University, Beijing 100871, China

²Collaborative Innovation Center of Atmospheric Environment and Equipment Technology, Nanjing University of Information Science & Technology, Nanjing 210044, China

³State Key Laboratory of Automotive Safety and Energy, Tsinghua University, Beijing 100084, China

⁴State Key Laboratory of Multiphase Complex Systems, Institute of Process Engineering, Chinese Academy of Sciences, Beijing 100190, China

⁵Beijing Innovation Center for Engineering Sciences and Advanced Technology, Peking University, Beijing 100871, China

⁶State Key Laboratory of Atmospheric Boundary Layer Physics and Atmospheric Chemistry (LAPC), Institute of Atmospheric Physics, Chinese Academy of Sciences, Beijing 100029, China

[§]These authors contributed equally to this work.

Correspondence to: Min Hu (minhu@pku.edu.cn).

ABSTRACT

Vehicle exhaust and cooking emissions are closely related to the daily life of city dwellers. Here, we defined the secondary organic aerosol (SOA) derived from vehicle exhaust and cooking emission as "Urban Lifestyle SOA", and simulated their formation using a Gothenburg potential aerosol mass reactor (Go: PAM). The vehicle exhaust and cooking emission were separately simulated, and their samples were defined as "vehicle group" and "cooking group", respectively. After samples had been aged under 0.3-5.5 days of equivalent photochemical age, these two urban lifestyle SOA showed markedly distinct features in SOA mass growth potentials, oxidation pathways, and mass spectra. The SOA/POA (primary organic aerosol) mass ratios of vehicle groups (107) were 44 times larger than those of cooking groups (2.38) at about 2 days of equivalent photochemical age, according to the measurement of scanning mobility particle sizer (SMPS). A high-resolution time-of-flight aerosol mass spectrometer was used to perform a deeper analysis. It reveals that organics from the vehicle may undergo the alcohol/peroxide and carboxylic acid oxidation pathway to produce abundant less/more oxidized oxygenated OA (LO-OOA and MO-OOA), and only a few primary hydrocarbon-like organic aerosol (HOA) remains unaged. In contrast, organics from cooking may undergo the alcohol/peroxide oxidation pathway to produce moderate LO-OOA, and comparable

primary cooking organic aerosol (COA) remains unaged. Our findings provide an insight into atmospheric contributions and chemical evolutions for urban lifestyle SOA, which would greatly influence the air quality and health risk assessments in urban areas.

1. Introduction

Organic aerosol (OA) contributes 20-90% of submicron aerosols in mass (Jimenez et al., 2009;Zhang et al., 2011), and its fraction in urban areas is higher than that in suburban or background (Zhou et al., 2020). The OA can be divided into the primary organic aerosol (POA) and the secondary organic aerosol (SOA). There are many potential sources of POA, such as coal combustion, biomass burning, vehicle exhaust, cooking procedure, and so forth (Jimenez et al., 2009;Zhang et al., 2011;Zhou et al., 2020). SOA is formed via the oxidation of gas-phase organics and the distribution between gas and particle phase (Donahue et al., 2009). Significant SOA formation has been observed in several urban areas, but models typically fail to simulate this phenomenon accurately (Matsui et al., 2009;Kleinman et al., 2008;Volkamer et al., 2006;de Gouw et al., 2008). This discrepancy may attribute to the limited knowledge about the sources and characteristics of urban SOA.

Over the past decades, megacities have already been widespread in developed regions, and rapid urbanizations have been sweeping across the globe especially in developing areas (Zhang et al., 2015). An increasing number of people tend to live in the urban for their livelihood, where they suffer from serious air pollution simultaneously from urban lifestyle sources typically involving vehicle and cooking fumes (An et al., 2019;Zhang et al., 2015;Chan and Yao, 2008;Guo et al., 2014;Guo et al., 2020). For instance, polycyclic aromatic hydrocarbons (PAHs) are important carcinogens coming from vehicle and cooking, which can cause severe lung cancer (Seow et al., 2000;Kim et al., 2015;Zhong et al., 1999). After PAHs are emitted to ambient air, they can be oxidized, distributed into particle phase, and finally become part of POA or SOA, thus adding unknown deviations on health risk assessments (Masuda et al., 2020).

Vehicle and cooking emissions are important sources of OA in urban areas (Rogge et al., 1991;Rogge et al., 1993;Hu et al., 2015;Hallquist et al., 2016;Crippa et al., 2013;Mohr et al., 2012;Guo et al., 2013;Guo et al., 2012), [take the megacity \(total population of its metro area is more than 3 M\) for example](#), in London, these two lifestyle sources contributed 50% of OA in average (Allan et al., 2010). In addition, the vehicle itself could even contribute 62% of OA mass in the rush hour of New York City (Sun et al., 2012). As for OA source appointments in Paris, vehicle and cooking contributed a maximum of 46-50% OA (Crippa et al., 2013). According to seasonal observations in Beijing, there were at least 30% of OA coming from the vehicle and cooking emissions (Hu et al., 2017). Briefly, these two urban lifestyle sources are closely related to the daily life of city residents and could account for 20-60% of ambient OA mass in urban areas when only considering their contributions to POA (Allan et al., 2010;Sun et al., 2011;Ge et al., 2012;Sun et al., 2012;Lee et al., 2015;Hu et al., 2017). Furthermore, the model speculated that vehicle and cooking emissions might even contribute over 90% of SOA in downtown Los Angeles by applying hypothetical parameters with a certain degree of uncertainty (Hayes et al., 2015). Therefore, vehicle and cooking are momentous sources of both POA and SOA in urban areas, and could be defined as “Urban Lifestyle Source of OA”.

As is well-known, large amounts of volatile, semi-volatile and intermediate-volatility organic compounds (VOCs,

SVOCs and IVOCs, respectively) are emitted from vehicle and cooking sources, leading to largely potential SOA productions (Klein et al., 2016; Katragadda et al., 2010; Liu et al., 2017c; Tang et al., 2019; Zhao et al., 2015; Esmaeilirad and Hosseini, 2018; Zhao et al., 2017; Yu et al., 2020). Laboratory studies have investigated the formation of vehicle or cooking SOA using a smog chamber or an oxidation flow reactor (OFR). On the one hand, some laboratory experiments have investigated the vehicle SOA based on variables such as fuel types, engine types, operating conditions, and so on (Deng et al., 2020; Suarez-Bertoa et al., 2015; Zhao et al., 2015; Du et al., 2018). Several smog chamber studies found that the mass loading of SOA exceeded POA when the equivalent photochemical age was more than one day (Gordon et al., 2013; Chirico et al., 2010; Nordin et al., 2013). Besides, OFR could simulate a higher OH exposure, and the peak SOA production occurred after 2-3 days of equivalent atmospheric oxidation (Tkacik et al., 2014; Zhao et al., 2018; Timonen et al., 2017; Watne et al., 2018; Alanen et al., 2017). The mass spectra of vehicle SOA showed both semi-volatile and low-volatility oxygenated organic aerosol (SV-OOA and LV-OOA) features along with the growth of oxidation degree (Tkacik et al., 2014). [NO_x levels may greatly influence the chemical evolution of vehicle SOA, and its NO_x/VOCs values are often strongly dependent on the sampling time and place in urban areas \(Zhan et al., 2021; Wei et al., 2014\). It is found that the photochemical ages for maximum SOA production under high-NO_x levels were lower than those under low-NO_x levels among OFR simulations \(Liao et al., 2021\).](#) On the other hand, only a few laboratory experiments have investigated the cooking SOA based on simplified ingredients or a single cooking method, involving heated cooking oils (Liu et al., 2017a; Liu et al., 2018), stir-frying spices (Liu et al., 2017b), charbroiled meat (Kaltsonoudis et al., 2017) and Chinese cuisines (Zhang et al., 2020b). These laboratory experiments indicated that the characteristics of SOA are influenced by multiple factors, such as cooking methods, fuels, cookers, or ingredients. The mass ratios of POA and SOA derived from cooking are comparable, and the mass spectra of SOA showed much more similarities with the ambient semi-volatile oxygenated OA (SV-OOA) factors (Liu et al., 2018). Although these laboratory studies have provided important insights into the secondary formation of the vehicle and cooking SOA, significant uncertainties still exist. Nobody has compared the different natures generated from these two urban lifestyle sources in detail, let alone pointed out their potentially different roles in the real atmosphere.

In this work, we have designed our vehicle and cooking laboratory experiments according to daily basis situations in urban areas of China. For vehicle exhaust simulation, China Phase V gasoline and three common operation conditions were chosen. For cooking emission simulation, four prevalent Chinese domestic cooking types were evaluated. A Gothenburg potential aerosol mass reactor (Go: PAM) was used as the oxidation system. All the fresh or aged OA was characterized in terms of mass growth potentials, elemental ratios, oxidation pathways, and mass spectra. The aged OA could be divided into POA and SOA. The latter was defined as “Urban Lifestyle SOA” whose mass spectra would be compared with those of ambient SOA, like less-oxidized oxygenated OA (LO-OOA) and more-oxidized oxygenated OA (MO-OOA) measured in urban areas of China. These findings aim to support the estimation of these two urban lifestyle SOA in ambient air, conducting to the policy formulation of pollution source control and health risk assessment of exposure to vehicle and cooking fumes.

2. Material and Method

2.1 Experimental Setup

The vehicle experiment was conducted from July to October in 2019, at the Department of Automotive Engineering, Tsinghua University. The cooking experiment was conducted from November 2019 to January 2020, at Langfang Branch, Institute of Process Engineering, Chinese Academy of Sciences. The laboratory simulations of two urban lifestyle SOA were conducted with the same oxidation and measurement system. Table 1-2 contains information on vehicle and cooking experiment conditions. The vehicle exhaust was emitted from a Gasoline direct engine (GDI) with China V gasoline (similar to Euro V) under three speeds (20, 40, 60 km/h), which represented the urban road condition in China (Zhang et al., 2020a). The commercial China Phase V gasoline was used as the fuel, which has equivalent octane number 92 level (RON 92), 10 ppm (v/v, max) sulfur, 25% (v/v, max) olefin, about 40% (v/v, max) aromatics, 2 mg/L Mn and no oxygenates (Yinhui et al., 2016). More information about the GDI engine can be found in Table S2-S3. For all experiments, the GDI engine ran in a single room, its exhaust was drawn into the pipeline and then entered the Go: PAM at a 30 fold dilution where aerosols and gases reacted at a stable temperature and relative humidity. On the other hand, four kinds of domestic cuisines were cooked with liquefied petroleum gas (LPG) in an iron wok, including deep-frying chicken, shallow-frying tofu, stir-frying cabbage, and Kung Pao chicken composed of cucumbers, peanuts, and chicken. The cooking time and oil temperature were different due to the inherent features of the ingredients. For all experiments, the closed kitchen was full of fumes where the vision was blurred and the air was choky after a long time of the cooking process. Subsequently, the cooking fumes were drawn into pipeline from a kitchen to a lab and then entered the Go: PAM at an 8 fold dilution where aerosols and gases reacted at a stable temperature and relative humidity. Both vehicle and cooking fumes were diluted at a constant ratio by a Dekati Dilutor (e-Diluter, Dekati Ltd.). *Vehicle exhaust from tailpipe was first diluted by a gradient heated dilution system (6 fold) and then diluted by an unheated dilution system (5 fold). The temperature of sample flow was near indoor temperature (20-25°C) after secondary dilution systems. The cooking fumes was collected through the kitchen ventilator, where the temperature was similar to that of indoor air.* The Go: PAM was able to produce high OH exposures using an ultraviolet lamp ($\lambda=254$ nm) in the presence of ozone and water vapor to simulate the photochemical oxidation in the atmosphere (Li et al., 2019a; Watne et al., 2018). The internal structure of Go: PAM can be found in Figure S1. Blank experiments were separately designed in the presence of boiling water or dilution air under the same condition. The OA concentrations of blank groups were far below those of experimental groups, which indicated the background values were minor (Table S1). More details about experimental design and instruments can be found in SI.

2.2 Measurements of the Gas and Particle Phase.

Figure 1 presents the design of this laboratory simulation. The gases and aerosols were emitted from the GDI room or kitchen, then reacted and sampled in a lab. The chemical compositions of OA were measured by a high-resolution time-of-flight aerosol mass spectrometer (HR-ToF-AMS, Aerodyne Research Inc.), in which the non-refractory particles including organics, sulfate, nitrate, ammonium, and chloride were instantly vaporized by a 600°C tungsten. Next, the vaporized

compounds were ionized by an electron impact (EI) ionization with 70 eV. Finally, the fragment ions were pulsed to a time-of-flight MS chamber and detected by the multi-channel plate detector (MCP). More information about HR-ToF-AMS is described in detail elsewhere (Nash et al., 2006; DeCarlo et al., 2006). In this study, its time resolution was 2 min (precisely, 1 min for a mass-sensitive V-mode, and 1 min for a high mass resolution W-mode). As for HR-ToF-AMS, the aged OA were those measured under certain OH exposure. Two sets of scanning mobility particle sizers (SMPS-1, Differential Mobility Analyzer, Electrostatic Classifier model 3080; Condensation Particle Counter model 3778; SMPS-2, Differential Mobility Analyzer, Electrostatic Classifier model 3082; Condensation Particle Counter model 3772; TSI Inc.) scanned every 2 min before and after Go: PAM individually to identify the size distribution and number concentration of particles. The SMPS-1 determined the mass concentration of POA, while the SMPS-2 determined the mass concentration of aged OA, and their mass difference could be regarded as the SOA. A SO₂ analyzer (Model 43i, Thermo Electron Corp.) was used to measure the decay of SO₂ in offline adjustment. The measured CO₂ concentrations (Model 410i, Thermo Electron Corp.) were used to conduct CO₂ correction for AMS data to reduce the CO₂ interference to organic fragments in mass spectra of HR-ToF-AMS. The particle densities were measured through the determination of the DMA-CPMA-CPC system (DMA-Differential Mobility Analyzer, Electrostatic Classifier model 3080, TSI Inc.; CPMA- Centrifugal Particle Mass Analyzer, version 1.53, Cambustion Ltd.; CPC- Condensation Particle Counter, Condensation Particle Counter model 3778, TSI Inc.). To prevent freshly warm gas from condensing on the pipe wall, sampling pipes were equipped with heat insulation cotton and a temperature controller. Silicon tubes were used to dry the emissions before they entered measuring instruments. Before each experiment, all pipelines and the Go: PAM chamber were continuously flushed with purified dry air, until the concentrations were minimal (just like blank groups in Table S1) when the UV was on or off. The SOA formed in each experiment represented the upper limit due to the presence of background concentration.

2.3 Data Analysis.

2.3.1 HR-ToF-AMS Data

The SQUIRREL 1.57 and PIKA 1.16 written in IGOR (Wavemetrics Incorporation, USA) were used to analyze the HR-ToF-AMS data including mass concentrations, elemental ratios, ion fragments, and mass spectra. The ionization efficiency (IE), relative ionization efficiency (RIE), and collection efficiency (CE) were determined individually before data processing. The 300 nm ammonium nitrate particles were applied for converting the instrument signals to actual mass concentrations (Jayne et al., 2000; Drewnick et al., 2005). Before the formal experiment, the IE and RIE_{SO4} were calculated by the comparison of HR-ToF-AMS and SMPS, when the sampling flow was generated by 300 nm ammonium nitrate and 300 nm ammonium sulfate, respectively, with an Aerosol generator (DMT Inc.). The CE was a fluctuant value influenced by the emission condition, so it was estimated by the comparison of HR-ToF-AMS (sampling after Go: PAM) and SMPS-2 (sampling after Go: PAM) during the formal experiment. The CE and RIE_{Org} were theoretically different in every emission or oxidation condition, so we directly use the SMPS measurements to determine the aged OA mass concentration. As for the cooking experiment, the IE value was 7.77×10^{-8} , the RIE_{SO4} was 1.4, the RIE_{Org} was 1.4 (default value, the fluctuation of RIE_{Org}

was included in CE), the average CE was about 0.55 (ranged from 0.3 to 0.7). As for the vehicle experiment, the IE value was 7.69×10^{-8} , the RIESO₄ was 1.3, the RIEOrg was 1.4 (default value, the fluctuation of RIEOrg was included in CE), the average CE was about 0.6 (ranged from 0.4 to 0.7). For some of the experimental groups, the mass spectra were resolved by positive matrix factorization (PMF) analysis to do deeper analyses (Ulbrich et al., 2009).

2.3.2 Determination and Evaluation of Oxidation Conditions in Go: PAM

The Go: PAM conditions for vehicle and cooking experiments could be seen in Table 3 and Table 4, respectively. Their experiment conditions (such as residence time and RH) were not completely the same because of the inherent difference and experimental design between two sources. Whereas, some comparisons could be still analyzed in the similar OH exposure, and their RH conditions were both low where photochemical oxidations instead of aqueous-phase processing dominated the chemical evolution process (Xu et al., 2017). The OH exposures and corresponding photochemical ages in Go: PAM were calculated through an offline adjustment based on the decay of SO₂ (Lambe et al., 2011). As shown in equation (1), K_{OH-SO_2} is the reaction rate constant of OH radical and SO₂ ($9.0 \times 10^{-13} \text{ molecule}^{-1} \cdot \text{cm}^3 \cdot \text{s}^{-1}$). The SO_{2,f} and SO_{2,i} are the SO₂ concentrations (ppb) under the conditions of UV lamp on or off respectively. The photochemical age (days) can be calculated in equation (2) when assuming the OH concentration is $1.5 \times 10^6 \text{ molecules} \cdot \text{cm}^{-3}$ in the atmosphere (Mao et al., 2009).

$$OH \text{ exposure} = \frac{-1}{K_{OH-SO_2}} \times \ln\left(\frac{SO_{2,f}}{SO_{2,i}}\right) \quad (1)$$

$$Photochemical \text{ age} = \frac{OH \text{ exposure}}{24 \times 3600 \times 1.5 \times 10^6} \quad (2)$$

Except for the off-line calibration based on the decay of SO₂, a flow reactor exposure estimator was also used in this study (Peng et al., 2016). The OH exposures calculated by these two methods showed a good correlation (Figure S2&S3). This estimator could also evaluate the potential non-OH reactions in the flow reactor such as the photolysis of VOCs, the reactions with O(¹D), O(³P), and O₃. The flow reactor exposure estimator showed that OH reactions played the dominant role in our experiments. It is found that the heterogeneous reaction of ozone with oleic acid aerosol particles was influenced by humidity and reaction time in an aerosol flow reactor (Vesna et al., 2009). Therefore, non-OH reactions, such as the ozonolysis of unsaturated fatty acids, may also be important in forming SOA, which missed specific designs in our experiment.

Furthermore, the external OH reactivity and OH exposure were both influenced by external OH reactants, such as NO_x and VOCs during experiments. The NO_x concentration was measured by a NO-NO₂-NO_x Analyzer (Model 42i, Thermo Electron Corporation, USA). As for VOCs, we have divided them into 5 types including alkane, alkene, aromatic, O-VOCs (Oxidized VOCs, mainly included aldehyde and ketone), and X-VOCs (halogenated-VOCs) using the measurement of GC-MS (Gas Chromatography-Mass Spectrometry, GC-7890, MS-5977, Agilent Technologies Inc). The compounds with relatively high proportion were regarded as surrogate species for each type of VOCs. The total concentrations of VOCs were determined by a portable TVOC Analyzer (PGM-7340, RAE SYSTEMS). The external OH reactivities for different vehicle experiments ($10.4 \sim 20.2 \text{ s}^{-1}$) were all comparable to that of off-line calibration results (15.8 s^{-1}), and the external OH reactivities

for different cooking experiments ($21.7\sim 25.7\text{ s}^{-1}$) were also comparable to that of off-line calibration results (24.0 s^{-1}). Besides, the ratio of OH exposure calculated by the estimator to that calculated by the decay of SO_2 ranged from 83% to 119% for vehicle experiments, and 97% to 111% for cooking experiments, which means that our off-line OH exposure could be a representative value to all experiments. Detailed tests about mixing condition and wall loss of the Go: PAM have been conducted in previous work according to Li et al. (Li et al., 2019a) and Watne et al. (Watne et al., 2018), which could be found in Figure S4. In this study, we still corrected the wall loss of particles in each size bin measured by two synchronous SMPS (two SMPS run before and after Go: PAM respectively). More details about Go: PAM can be found in SI.

3. Result and Discussion

3.1 Secondary Formation Potential of the Urban Lifestyle OA.

As Figure 2 shows, the mass growth potentials of two urban lifestyle OA were quite different. The mass growth potentials were represented by SOA/POA mass ratios. The SMPS-1 determined the mass concentration of POA, while the SMPS-2 determined the mass concentration of aged OA, and their mass difference could be regarded as the SOA. Their SOA/POA mass ratios both increased gradually and finally reached the peak after 2-3 days of equivalent photochemical age, and the overall SOA mass growth potentials of vehicle SOA were far larger than those of cooking SOA. When the equivalent photochemical age was near 2 days (1.7 days), the mass growth potentials of vehicle SOA ranged from 83 to 150. In contrast, the mass growth potentials of cooking SOA only ranged from 1.8 to 3.2 at about 2.1 days. Even if there was still a slight growth trend for cooking SOA at the highest OH exposure, it surely exhibited a much weaker mass growth potential on the whole compared with that of vehicle SOA. This significant distinction indicated that the vehicle exhaust may contribute abundant SOA and relatively fewer POA, while cooking emission may produce moderate POA and SOA in the atmosphere, which could attribute to their different types of gaseous precursors. Interestingly, a similar phenomenon had been observed from an OFR simulation in the urban roadside of [Hong Kong](#), where potential SOA from motor vehicle exhaust was much larger than primary HOA, while potential SOA from cooking emission was comparable to primary COA (Liu et al., 2019).

3.2 Secondary Formation Pathway of the Urban Lifestyle OA.

As Figure 3 shows, the evolution of O:C molar ratios (O/C) of two urban lifestyle OA were quite different. Although their oxidation degrees both increased gradually and finally reached the peak after 2-3 days of equivalent photochemical age, the O/C values of aged vehicle OA were far larger than those of aged cooking OA. When the equivalent photochemical age was 0.6 day, the O/C of aged vehicle OA was 0.4-0.5, resembling a kind of LO-OOA in ambient air. When the equivalent photochemical age was near 2 days (1.7 days), the O/C of aged vehicle OA could reach 0.6, which was almost like a type of MO-OOA in the atmosphere. In contrast, the O/C of aged cooking OA only rose to 0.4 at 2.1 days, similar to a kind of LO-OOA. These distinct features of O/C suggested that aged vehicle OA was divided into LO-OOA and MO-OOA under different oxidation conditions, while the aged cooking OA was only composed of LO-OOA. This difference was probably related to their precursors.

Figure 4 illustrates diverse oxidation pathways of various sources of OA in a Van Krevelen diagram (Heald et al.,

2010;Ng et al., 2011;Presto et al., 2014). The cooking groups fell along a line with a slope of -0.10 implying an alcohol/peroxide pathway in forming SOA, while the vehicle groups fell along a line with a slope of -0.55 implying an oxidation pathway between alcohol/peroxide and carboxylic acid reaction. Additionally, these two secondary evolution properties are both different from those of biomass burning OA (slope \sim -0.6) (Lim et al., 2019) and ambient OA (slope \sim -1 to -0.5) (Heald et al., 2010;Hu et al., 2017;Ng et al., 2011), indicating that these two urban lifestyles SOA may undergo distinct oxidation pathways.

3.3 Characteristics in Mass Spectra of the Urban Lifestyle OA.

As shown in Figure 5, the signal fraction of organic fragments at m/z 43 (f_{43}) and m/z 44 (f_{44}) has been widely adopted to represent the oxidation process of OA (Ng et al., 2010;Hennigan et al., 2011). Generally, f_{43} and f_{44} derive from oxygen-containing fragments, the former comes from less oxidized components while the latter comes from more oxidized ones. The datasets of vehicle and cooking groups fell along in different regions and showed different variations in the plot. Almost all aged cooking OA displayed relatively lower f_{44} and higher f_{43} , and its f_{43} and f_{44} both increased slightly with the growing OH exposure, eventually distributing in the LO-OOA region. In contrast, all aged vehicle OA displayed moderate f_{43} and abundant f_{44} , and only its f_{44} showed an obvious souring with the growing OH exposure, initially distributing in the LO-OOA region but finally spreading near the MO-OOA region. These distinct evolutions of oxygen-containing fragments for two urban lifestyle OA inferred their intrinsic oxidation pathways and precursors.

Figure 6 and Table 5 depict mass spectra and prominent peaks of aged OA from two urban lifestyle sources which could be used to deduce their inherent properties (Zhang et al., 2005;Kaltsonoudis et al., 2017;Liu et al., 2018;Chirico et al., 2010;Nordin et al., 2013;Zhang et al., 2020b). The maximum SOA mass growth potentials of aged cooking OA only ranged from 1.9-3.2 implying a mixture of POA and SOA, so its mass spectra needed to be deeply resolved by PMF to separate the POA and SOA (precisely, a kind of LO-OOA). Generally, there is at least one POA and one SOA (factor 1-POA; factor 2-SOA). When three or more factors were set, it was found that elemental ratios or mass spectra of additional OA factors are quite similar to factor 1 or factor 2, which means that it was hard to find another new OA factor. Therefore, 2 OA factors were finally set, one for POA and another for SOA. As Figure S5-S8 shows, the SOA factors present a larger fraction of oxygen-containing fragments (especially in m/z 28, 29, 43, 44) and higher O/C, which is significantly different from those POA factors. Whereas, those mass growth potentials of aged vehicle OA were extremely high, suggesting that it was fully oxidized and almost composed of SOA. According to the O/C ratios, the vehicle SOA under 0.6 day of photochemical age was defined as vehicle LO-OOA, while that under 2.9 days was regarded as vehicle MO-OOA.

For average vehicle LO-OOA mass spectra, the prominent peaks were m/z 43 ($f_{43}=0.133\pm0.003$), 44 ($f_{44}=0.077\pm0.001$), 29 ($f_{29}=0.076\pm0.003$), 28 ($f_{28}=0.066\pm0.001$), 41 ($f_{41}=0.051\pm0.005$), and 55 ($f_{55}=0.043\pm0.004$) dominated by $C_2H_3O^+$, $C_3H_7^+$, CO_2^+ , CHO^+ , $C_2H_5^+$, CO^+ , $C_3H_5^+$, $C_3H_3O^+$, and $C_4H_7^+$ respectively, while the prominent peaks of average vehicle MO-OOA were m/z 44 ($f_{44}=0.146\pm0.060$), 28 ($f_{28}=0.134\pm0.062$), 43 ($f_{43}=0.117\pm0.033$), 29 ($f_{29}=0.071\pm0.014$), 45 ($f_{45}=0.032\pm0.007$), and 27 ($f_{27}=0.030\pm0.009$) dominated by CO_2^+ , CO^+ , $C_2H_3O^+$, CHO^+ , $C_2H_5^+$, CHO_2^+ , $C_2H_5O^+$, and $C_2H_3^+$ respectively.

263 Compared with vehicle SOA mass spectra from other studies (Table 5), our average GDI SOA (LO-OOA and MO-OOA)
264 illustrated more abundances of oxygen-containing ions than those of Gasoline SOA and Diesel SOA simulated by a smog
265 chamber with lower OH exposures (Chirico et al., 2010;Nordin et al., 2013).

266 For average cooking LO-OOA, it was less oxidized than those from vehicle groups, whose prominent peaks were m/z
267 43 ($f_{43}=0.097\pm0.008$), 44 ($f_{44}=0.065\pm0.010$), 29 ($f_{29}=0.065\pm0.013$), 41 ($f_{41}=0.058\pm0.008$), 55 ($f_{55}=0.056\pm0.006$), and 28
268 ($f_{28}=0.053\pm0.011$) dominated by $C_2H_3O^+$, $C_3H_7^+$, CO_2^+ , CHO^+ , $C_2H_5^+$, $C_3H_5^+$, $C_3H_3O^+$, $C_4H_7^+$, and CO^+ respectively.
269 Compared with other cooking SOA mass spectra (Table 5), our average cooking LO-OOA had similar peaks with heated oil
270 SOA but was different from that meat charbroiling SOA which displayed much more hydrocarbon-like features (Liu et al.,
271 2018;Kaltsonoudis et al., 2017).

272 3.4 Potential Chemical Evolution of Urban Lifestyle OA in the Atmosphere.

273 The AMS mass spectra indicated that the chemical evolution of urban lifestyle OA in the Go: PAM might provide new
274 insights and references on those of ambient OA observed in the atmosphere. Figure 7 plots the correlation coefficients between
275 the laboratory aged OA and ambient PMF-OA factors with growing photochemical ages (Li et al., 2020a). The field study
276 was deployed at the Institute of Atmospheric Physics (IAP), Chinese Academy of Sciences (39°58'N; 116°22'E) in autumn
277 and winter (Autumn: Oct. 1st, 2018 – Nov. 15th, 2018; Winter: Jan. 5th, 2019 – Jan. 31st, 2019) (Li et al., 2020a). The sample
278 site is located in the south of Beitucheng West Road and west of [Beijing-Chengde](#) expressway in Beijing, which is a typical
279 urban site affected by local emissions (Li et al., 2020b). Table 6 exhibits correlations of mass spectra between laboratory
280 results and ambient PMF factors, where the aged laboratory cooking OA was divided into POA and LO-OOA while the
281 laboratory vehicle OA was divided into LO-OOA and MO-OOA.

282 For the aged GDI OA in Figure 7, its average mass spectra remained some ambient HOA features (Pearson $r=0.80$) under
283 low photochemical age of 0.6 day with moderate hydrocarbon-like ions such as m/z 41 and 55, but it had already reached the
284 same oxidation degree of ambient LO-OOA (Pearson $r=0.81$) with high O/C (0.46) and f_{43} (0.133). After aging in the Go:
285 PAM, the aged OA might finally become a kind of ambient MO-OOA (Pearson $r=0.97$) at 5.1 days of photochemical age.
286 This evolution of GDI OA (from HOA to LO-OOA to MO-OOA) was similar to the result of a previous vehicle OA simulation
287 (from HOA to SV-OOA to LV-OOA) (Tkacik et al., 2014).

288 For the aged cooking OA in Figure 7, although its correlations with ambient LO-OOA increased gradually from 0.56 to
289 0.73 along with the growing photochemical ages, its correlations with ambient COA kept a high level all the time (Pearson
290 $r>0.81$) implying a mixture of POA and SOA due to some hardly oxidized compounds emitted from the cooking process.
291 Therefore, it is necessary to resolve aged cooking OA mass spectra deeply by PMF (Figures S4-S11) and then compared its
292 laboratory PMF results with ambient PMF factors. As Table 6 shows, the laboratory cooking POA was similar to ambient
293 COA (Pearson $r=0.86$) but less likely to LO-OOA (Pearson $r=0.46$) or MO-OOA (Pearson $r=0.39$). By contrast, the laboratory
294 cooking LO-OOA displayed many more ambient LO-OOA features (Pearson $r=0.76$) and relatively fewer ambient COA
295 characteristics than laboratory cooking POA did. In short, these comparisons between laboratory and ambient results revealed

that organics from these two urban lifestyle sources might eventually form different SOA types in the real atmosphere.

4. Conclusion

In the present work, we define two urban lifestyle SOA in details and investigate their mass growth potentials, formation pathways, mass spectra, and chemical evolutions comprehensively. At about 2 days of equivalent photochemical age, the SOA/POA mass ratios of vehicle groups (107) were 44 times larger than those of cooking groups (2.38), and the O: C molar ratios of vehicle groups (0.66) was about 2 times large as those of cooking groups (0.34). Besides, both vehicle and cooking groups may undergo an alcohol/peroxide pathway to form LO-OOA, and the vehicle groups extra undergo a carboxylic acid pathway to form part of MO-OOA. Furthermore, the characteristic mass spectra of these two urban lifestyle SOA could provide necessary references to estimate their mass fractions in ambient air, through a multilinear engine model (ME-2) (Canonaco et al., 2013;Qin et al., 2017). This application would reduce the large gaps of total atmospheric contributions and relevant environment effects for urban SOA, although remaining several uncertainties on SOA mass spectra due to missing complex mixture conditions in the Go: PAM.

There are some uncertainties of our Go: PAM simulation. We focused more on the photochemical oxidation of SOA under low RH levels, but aqueous-phase processing at high RH levels may also have impacts to SOA production. In the future, it'll be better to strictly control the RH, high/low NO_x or SO₂, additional inorganic seeds, and so forth, to deeply investigate how the aerosol ages as a function of equivalent days of atmospheric oxidation. S/I VOCs may play important roles in forming SOA but were indeed partly lost in pipelines, and its sampling and quantification are really hard and challenging, which needs more sophisticated experimental design. Moreover, contribution of ozonolysis to SOA formation should be individually studied in further research. Besides, it is recommended to add humidity to the carrier gas and turn on the lights during the OFR cleanout stage, in order to minimize the background concentration in the Go: PAM.

Although strict policies have been implemented to reduce primary particulate matter (PM) in urban areas. However, secondary PM especially for the abundant and complicated SOA, is difficult to be restricted (Wu et al., 2017;Li et al., 2018). According to our results, on the one hand, vehicle SOA might be a mixture of both LO-OOA and MO-OOA with high secondary formation potential, so it would be better not only filter out the exhaust PM with Gasoline Particulate Filter (GPF) but also reduce the gaseous precursors to restrict the secondary formation. On the other hand, cooking SOA might be a kind of LO-OOA with relatively low secondary formation potential, so it could be enough to remove the gas and particle emissions at the same level. In the future, these two urban lifestyle SOA may present increasing contributions in urban areas especially in megacities with growing atmospheric oxidants (Li et al., 2019b;Wang et al., 2017;Li et al., 2020a;Li et al., 2020b), but their investigations and further managements are far from sufficient, making it possible to become a greatly meaningful research focus.

Data availability. The data provided in this paper can be obtained from the author upon request (minhu@pku.edu.cn).

Supplement. An independent supplement document is available.

Authorship contributions. Zirui Zhang: Investigation, Data curation, Methodology, Formal analysis, Writing - original draft, Writing - review & editing. Wenfei Zhu: Investigation, Data curation, Methodology, Formal analysis, Writing - review & editing. Min Hu: Project administration, Supervision, Funding acquisition, Writing - review & editing. Kefan Liu: Investigation, Data curation, Formal analysis. Hui Wang: Investigation, Data curation. Rongzhi Tang Investigation, Data curation. Ruizhe Shen: Investigation, Data curation. Ying Yu: Investigation, Data curation. Rui Tan: Investigation, Data curation. Kai Song: Investigation, Data curation. Yuanju Li: Investigation, Data curation. Wenbin Zhang: Investigation, Data curation. Zhou Zhang: Investigation, Data curation. Hongming Xu: Data curation. Shijin Shuai: Data curation. Shuangde Li: Data curation. Yunfa Chen: Data curation. Jiayun Li: Data curation. Yuesi Wang: Data curation. Song Guo: Project administration, Funding acquisition, Writing - review & editing.

Note: Zirui Zhang and Wenfei Zhu contributed equally to this work.

Competing interests. The authors declare that they have no known competing financial interests or personal relationships that could have appeared to influence the work reported in this paper.

Acknowledgements. Thanks to all authors from PKU who had directly participate in the main laboratory simulation. Thanks to all authors from THU and CAS who had provided the necessary experiment sites, instruments and data support.

Financial support. The research has been supported by the National Key R&D Program of China (2016YFC0202000), the National Natural Science Foundation of China (51636003, 91844301, 41977179, and 21677002), Beijing Municipal Science and Technology Commission (Z201100008220011), Open Research Fund of State Key Laboratory of Multiphase Complex Systems (MPCS-2019-D-09), and China Postdoctoral Science Foundation (2020M680242).

REFERENCES

- Alanen, J., Simonen, P., Saarikoski, S., Timonen, H., Kangasniemi, O., Saukko, E., Hillamo, R., Lehtoranta, K., Murtonen, T., Vesala, H., Keskinen, J., and Rönkkö, T.: Comparison of primary and secondary particle formation from natural gas engine exhaust and of their volatility characteristics, *Atmospheric Chemistry and Physics*, 17, 8739-8755, 10.5194/acp-17-8739-2017, 2017.
- Allan, J. D., Williams, P. I., Morgan, W. T., Martin, C. L., Flynn, M. J., Lee, J., Nemitz, E., Phillips, G. J., Gallagher, M. W., and Coe, H.: Contributions from transport, solid fuel burning and cooking to primary organic aerosols in two UK cities, *Atmospheric Chemistry And Physics*, 10, 647-668, 10.5194/acp-10-647-2010, 2010.
- An, Z., Huang, R. J., Zhang, R., Tie, X., Li, G., Cao, J., Zhou, W., Shi, Z., Han, Y., Gu, Z., and Ji, Y.: Severe haze in northern China: A synergy of anthropogenic emissions and atmospheric processes, *Proceedings of the National Academy of Sciences of the United States of America*, 116, 8657-8666, 10.1073/pnas.1900125116, 2019.
- Canonaco, F., Crippa, M., Slowik, J. G., Baltensperger, U., and Prévôt, A. S. H.: SoFi, an IGOR-based interface for the efficient use of the generalized multilinear engine (ME-2) for the source apportionment: ME-2 application to aerosol mass spectrometer data,

Atmospheric Measurement Techniques, 6, 3649-3661, 10.5194/amt-6-3649-2013, 2013.

Chan, C. K., and Yao, X.: Air pollution in mega cities in China, *Atmospheric Environment*, 42, 1-42, 10.1016/j.atmosenv.2007.09.003, 2008.

Chirico, R., DeCarlo, P. F., Heringa, M. F., Tritscher, T., Richter, R., Prevot, A. S. H., Dommen, J., Weingartner, E., Wehrle, G., Gysel, M., Laborde, M., and Baltensperger, U.: Impact of aftertreatment devices on primary emissions and secondary organic aerosol formation potential from in-use diesel vehicles: results from smog chamber experiments, *Atmospheric Chemistry And Physics*, 10, 11545-11563, 10.5194/acp-10-11545-2010, 2010.

Crippa, M., DeCarlo, P. F., Slowik, J. G., Mohr, C., Heringa, M. F., Chirico, R., Poulain, L., Freutel, F., Sciare, J., Cozic, J., Di Marco, C. F., Elsasser, M., Nicolas, J. B., Marchand, N., Abidi, E., Wiedensohler, A., Drewnick, F., Schneider, J., Borrmann, S., Nemitz, E., Zimmermann, R., Jaffrezo, J. L., Prevot, A. S. H., and Baltensperger, U.: Wintertime aerosol chemical composition and source apportionment of the organic fraction in the metropolitan area of Paris, *Atmospheric Chemistry And Physics*, 13, 961-981, 10.5194/acp-13-961-2013, 2013.

de Gouw, J. A., Brock, C. A., Atlas, E. L., Bates, T. S., Fehsenfeld, F. C., Goldan, P. D., Holloway, J. S., Kuster, W. C., Lerner, B. M., Matthew, B. M., Middlebrook, A. M., Onasch, T. B., Peltier, R. E., Quinn, P. K., Senff, C. J., Stohl, A., Sullivan, A. P., Trainer, M., Warneke, C., Weber, R. J., and Williams, E. J.: Sources of particulate matter in the northeastern United States in summer: 1. Direct emissions and secondary formation of organic matter in urban plumes, *Journal of Geophysical Research*, 113, 10.1029/2007jd009243, 2008.

DeCarlo, P. F., Kimmel, J. R., Trimborn, A., Northway, M. J., Jayne, J. T., Aiken, A. C., Gonin, M., Fuhrer, K., Horvath, T., Docherty, K. S., Worsnop, D. R., and Jimenez, J. L.: Field-deployable, high-resolution, time-of-flight aerosol mass spectrometer, *Analytical chemistry*, 78, 8281-8289, 10.1021/ac061249n, 2006.

Deng, W., Fang, Z., Wang, Z., Zhu, M., Zhang, Y., Tang, M., Song, W., Lowther, S., Huang, Z., Jones, K., Peng, P., and Wang, X.: Primary emissions and secondary organic aerosol formation from in-use diesel vehicle exhaust: Comparison between idling and cruise mode, *The Science of the total environment*, 699, 134357, 10.1016/j.scitotenv.2019.134357, 2020.

Donahue, N. M., Robinson, A. L., and Pandis, S. N.: Atmospheric organic particulate matter: From smoke to secondary organic aerosol, *Atmospheric Environment*, 43, 94-106, 10.1016/j.atmosenv.2008.09.055, 2009.

Drewnick, F., Hings, S. S., DeCarlo, P., Jayne, J. T., Gonin, M., Fuhrer, K., Weimer, S., Jimenez, J. L., Demerjian, K. L., Borrmann, S., and Worsnop, D. R.: A New Time-of-Flight Aerosol Mass Spectrometer (TOF-AMS)—Instrument Description and First Field Deployment, *Aerosol Science and Technology*, 39, 637-658, 10.1080/02786820500182040, 2005.

Du, Z., Hu, M., Peng, J., Zhang, W., Zheng, J., Gu, F., Qin, Y., Yang, Y., Li, M., Wu, Y., Shao, M., and Shuai, S.: Comparison of primary aerosol emission and secondary aerosol formation from gasoline direct injection and port fuel injection vehicles, *Atmospheric Chemistry and Physics*, 18, 9011-9023, 10.5194/acp-18-9011-2018, 2018.

Esmacilrad, S., and Hosseini, V.: Modeling the formation of traditional and non-traditional secondary organic aerosols from in-use, on-road gasoline and diesel vehicles exhaust, *Journal of Aerosol Science*, 124, 68-82, 10.1016/j.jaerosci.2018.07.003, 2018.

Ge, X., Setyan, A., Sun, Y., and Zhang, Q.: Primary and secondary organic aerosols in Fresno, California during wintertime: Results from high resolution aerosol mass spectrometry, *Journal of Geophysical Research: Atmospheres*, 117, n/a-n/a, 10.1029/2012jd018026, 2012.

Gordon, T. D., Tkacik, D. S., Presto, A. A., Zhang, M., Jathar, S. H., Nguyen, N. T., Massetti, J., Truong, T., Cicero-Fernandez, P., Maddox, C., Rieger, P., Chattopadhyay, S., Maldonado, H., Maricq, M. M., and Robinson, A. L.: Primary gas- and particle-phase emissions and secondary organic aerosol production from gasoline and diesel off-road engines, *Environmental science & technology*, 47, 14137-14146, 10.1021/es403556e, 2013.

Guo, S., Hu, M., Guo, Q., Zhang, X., Zheng, M., Zheng, J., Chang, C. C., Schauer, J. J., and Zhang, R.: Primary sources and secondary formation of organic aerosols in Beijing, China, *Environmental science & technology*, 46, 9846-9853, 10.1021/es2042564, 2012.

Guo, S., Hu, M., Guo, Q., Zhang, X., Schauer, J. J., and Zhang, R.: Quantitative evaluation of emission controls on primary and secondary organic aerosol sources during Beijing 2008 Olympics, *Atmospheric Chemistry and Physics*, 13, 8303-8314, 10.5194/acp-13-8303-2013, 2013.

Guo, S., Hu, M., Zamora, M. L., Peng, J. F., Shang, D. J., Zheng, J., Du, Z. F., Wu, Z., Shao, M., Zeng, L. M., Molina, M. J., and Zhang, R. Y.: Elucidating severe urban haze formation in China, *Proceedings of the National Academy of Sciences of the United States of America*, 111, 17373-17378, 10.1073/pnas.1419604111, 2014.

Guo, S., Hu, M., Peng, J. F., Wu, Z. J., Zamora, M. L., Shang, D. J., Du, Z. F., Zheng, J., Fang, X., Tang, R. Z., Wu, Y. S., Zeng, L. M., Shuai, S. J., Zhang, W. B., Wang, Y., Ji, Y. M., Li, Y. X., Zhang, A. L., Wang, W. G., Zhang, F., Zhao, J. Y., Gong, X. L., Wang, C. Y., Molina, M. J., and Zhang, R. Y.: Remarkable nucleation and growth of ultrafine particles from vehicular exhaust, *Proceedings of the National Academy of Sciences of the United States of America*, 117, 3427-3432, 10.1073/pnas.1916366117, 2020.

Hallquist, M., Munthe, J., Hu, M., Wang, T., Chan, C. K., Gao, J., Boman, J., Guo, S., Hallquist, A. M., Mellqvist, J., Moldanova, J., Pathak, R. K., Pettersson, J. B. C., Pleijel, H., Simpson, D., and Thynell, M.: Photochemical smog in China: scientific challenges and implications for air-quality policies, *Natl. Sci. Rev.*, 3, 401-403, 10.1093/nsr/nww080, 2016.

Hayes, P. L., Carlton, A. G., Baker, K. R., Ahmadov, R., Washenfelter, R. A., Alvarez, S., Rappenglück, B., Gilman, J. B., Kuster, W. C., de Gouw, J. A., Zotter, P., Prévôt, A. S. H., Szidat, S., Kleindienst, T. E., Offenberg, J. H., Ma, P. K., and Jimenez, J. L.: Modeling the formation and aging of secondary organic aerosols in Los Angeles during CalNex 2010, *Atmospheric Chemistry and Physics*, 15, 5773-5801, 10.5194/acp-15-5773-2015, 2015.

Heald, C. L., Kroll, J. H., Jimenez, J. L., Docherty, K. S., DeCarlo, P. F., Aiken, A. C., Chen, Q., Martin, S. T., Farmer, D. K., and Artaxo, P.: A simplified description of the evolution of organic aerosol composition in the atmosphere, *Geophysical Research Letters*, 37, 10.1029/2010gl042737, 2010.

Hennigan, C. J., Miracolo, M. A., Engelhart, G. J., May, A. A., Presto, A. A., Lee, T., Sullivan, A. P., McMeeking, G. R., Coe, H., Wold, C. E., Hao, W. M., Gilman, J. B., Kuster, W. C., de Gouw, J., Schichtel, B. A., Collett, J. L., Kreidenweis, S. M., and Robinson, A. L.: Chemical and physical transformations of organic aerosol from the photo-oxidation of open biomass burning emissions in an environmental chamber, *Atmospheric Chemistry and Physics*, 11, 7669-7686, 10.5194/acp-11-7669-2011, 2011.

Hu, M., Guo, S., Peng, J. F., and Wu, Z. J.: Insight into characteristics and sources of PM_{2.5} in the Beijing-Tianjin-Hebei region, China, *Natl. Sci. Rev.*, 2, 257-258, 10.1093/nsr/nwv003, 2015.

Hu, W., Hu, M., Hu, W. W., Zheng, J., Chen, C., Wu, Y. S., and Guo, S.: Seasonal variations in high time-resolved chemical compositions, sources, and evolution of atmospheric submicron aerosols in the megacity Beijing, *Atmospheric Chemistry And Physics*, 17, 9979-10000, 10.5194/acp-17-9979-2017, 2017.

Jayne, J. T., Leard, D. C., Zhang, X., Davidovits, P., Smith, K. A., Kolb, C. E., and Worsnop, D. R.: Development of an Aerosol Mass Spectrometer for Size and Composition Analysis of Submicron Particles, *Aerosol Science and Technology*, 33, 49-70, 10.1080/027868200410840, 2000.

Jimenez, J. L., Canagaratna, M. R., Donahue, N. M., Prevot, A. S., Zhang, Q., Kroll, J. H., DeCarlo, P. F., Allan, J. D., Coe, H., Ng, N. L., Aiken, A. C., Docherty, K. S., Ulbrich, I. M., Grieshop, A. P., Robinson, A. L., Duplissy, J., Smith, J. D., Wilson, K. R., Lanz, V. A., Hueglin, C., Sun, Y. L., Tian, J., Laaksonen, A., Raatikainen, T., Rautiainen, J., Vaattovaara, P., Ehn, M., Kulmala, M., Tomlinson, J. M., Collins, D. R., Cubison, M. J., Dunlea, E. J., Huffman, J. A., Onasch, T. B., Alfarra, M. R., Williams, P. I., Bower, K., Kondo, Y., Schneider, J., Drewnick, F., Borrmann, S., Weimer, S., Demerjian, K., Salcedo, D., Cottrell, L., Griffin, R., Takami, A., Miyoshi, T., Hatakeyama, S., Shimojo, A., Sun, J. Y., Zhang, Y. M., Dzepina, K., Kimmel, J. R., Sueper, D., Jayne, J. T., Herndon, S. C., Trimborn, A. M., Williams, L. R., Wood, E. C., Middlebrook, A. M., Kolb, C. E., Baltensperger, U., and Worsnop, D. R.: Evolution of organic aerosols in the atmosphere, *Science*, 326, 1525-1529, 10.1126/science.1180353, 2009.

Kaltsonoudis, C., Kostenidou, E., Louvaris, E., Psichoudaki, M., Tsiligiannis, E., Florou, K., Liangou, A., and Pandis, S. N.: Characterization of fresh and aged organic aerosol emissions from meat charbroiling, *Atmospheric Chemistry and Physics*, 17, 7143-7155, 10.5194/acp-17-7143-2017, 2017.

Katragadda, H. R., Fullana, A., Sidhu, S., and Carbonell-Barrachina, Á. A.: Emissions of volatile aldehydes from heated cooking oils, *Food Chemistry*, 120, 59-65, 10.1016/j.foodchem.2009.09.070, 2010.

Kim, C., Gao, Y. T., Xiang, Y. B., Barone-Adesi, F., Zhang, Y., Hosgood, H. D., Ma, S., Shu, X. O., Ji, B. T., Chow, W. H., Seow, W. J., Bassig, B., Cai, Q., Zheng, W., Rothman, N., and Lan, Q.: Home kitchen ventilation, cooking fuels, and lung cancer risk in a prospective cohort of never smoking women in Shanghai, China, *International journal of cancer*, 136, 632-638, 10.1002/ijc.29020, 2015.

Klein, F., Platt, S. M., Farren, N. J., Detournay, A., Bruns, E. A., Bozzetti, C., Daellenbach, K. R., Kilic, D., Kumar, N. K., Pieber, S. M., Slowik, J. G., Temime-Roussel, B., Marchand, N., Hamilton, J. F., Baltensperger, U., Prevot, A. S., and El Haddad, I.: Characterization of Gas-Phase Organics Using Proton Transfer Reaction Time-of-Flight Mass Spectrometry: Cooking Emissions, *Environmental science & technology*, 50, 1243-1250, 10.1021/acs.est.5b04618, 2016.

Kleinman, L. I., Springston, S. R., Daum, P. H., Lee, Y. N., Nunnermacker, L. J., Senum, G. I., Wang, J., Weinstein-Lloyd, J., Alexander, M. L., Hubbe, J., Ortega, J., Canagaratna, M. R., and Jayne, J.: The time evolution of aerosol composition over the

Mexico City plateau, *Atmospheric Chemistry And Physics*, 8, 1559-1575, 10.5194/acp-8-1559-2008, 2008.

Lambe, A. T., Ahern, A. T., Williams, L. R., Slowik, J. G., Wong, J. P. S., Abbatt, J. P. D., Brune, W. H., Ng, N. L., Wright, J. P., Croasdale, D. R., Worsnop, D. R., Davidovits, P., and Onasch, T. B.: Characterization of aerosol photooxidation flow reactors: heterogeneous oxidation, secondary organic aerosol formation and cloud condensation nuclei activity measurements, *Atmospheric Measurement Techniques*, 4, 445-461, 10.5194/amt-4-445-2011, 2011.

Lee, B. P., Li, Y. J., Yu, J. Z., Louie, P. K. K., and Chan, C. K.: Characteristics of submicron particulate matter at the urban roadside in downtown Hong Kong-Overview of 4 months of continuous high-resolution aerosol mass spectrometer measurements, *Journal of Geophysical Research: Atmospheres*, 120, 7040-7058, 10.1002/2015jd023311, 2015.

Li, J., Li, X.-B., Li, B., and Peng, Z.-R.: The Effect of Nonlocal Vehicle Restriction Policy on Air Quality in Shanghai, *Atmosphere*, 9, 299, 10.3390/atmos9080299, 2018.

Li, J., Liu, Q., Li, Y., Liu, T., Huang, D., Zheng, J., Zhu, W., Hu, M., Wu, Y., Lou, S., Hallquist, Å. M., Hallquist, M., Chan, C. K., Canonaco, F., Prévôt, A. S. H., Fung, J. C. H., Lau, A. K. H., and Yu, J. Z.: Characterization of Aerosol Aging Potentials at Suburban Sites in Northern and Southern China Utilizing a Potential Aerosol Mass (Go:PAM) Reactor and an Aerosol Mass Spectrometer, *Journal of Geophysical Research: Atmospheres*, 124, 5629-5649, 10.1029/2018jd029904, 2019a.

Li, J., Gao, W., Cao, L., Xiao, Y., Zhang, Y., Zhao, S., Liu, Z., Liu, Z., Tang, G., Ji, D., bo, H., Song, T., He, L., Hu, M., and Wang, Y.: Significant changes in autumn and winter aerosol composition and sources in Beijing from 2012 to 2018: effects of clean air actions, *Environmental pollution*, 115855, 10.1016/j.envpol.2020.115855, 2020a.

Li, J., Liu, Z., Gao, W., Tang, G., Hu, B., Ma, Z., and Wang, Y.: Insight into the formation and evolution of secondary organic aerosol in the megacity of Beijing, China, *Atmospheric Environment*, 220, 117070, 10.1016/j.atmosenv.2019.117070, 2020b.

Li, K., Jacob, D. J., Liao, H., Shen, L., Zhang, Q., and Bates, K. H.: Anthropogenic drivers of 2013-2017 trends in summer surface ozone in China, *Proceedings of the National Academy of Sciences of the United States of America*, 116, 422-427, 10.1073/pnas.1812168116, 2019b.

Liao, K., Chen, Q., Liu, Y., Li, Y. J., Lambe, A. T., Zhu, T., Huang, R. J., Zheng, Y., Cheng, X., Miao, R., Huang, G., Khuzestani, R. B., and Jia, T.: Secondary Organic Aerosol Formation of Fleet Vehicle Emissions in China: Potential Seasonality of Spatial Distributions, *Environmental science & technology*, 55, 7276-7286, 10.1021/acs.est.0c08591, 2021.

Lim, C. Y., Hagan, D. H., Coggon, M. M., Koss, A. R., Sekimoto, K., de Gouw, J., Warneke, C., Cappa, C. D., and Kroll, J. H.: Secondary organic aerosol formation from the laboratory oxidation of biomass burning emissions, *Atmospheric Chemistry And Physics*, 19, 12797-12809, 10.5194/acp-19-12797-2019, 2019.

Liu, T., Li, Z., Chan, M., and Chan, C. K.: Formation of secondary organic aerosols from gas-phase emissions of heated cooking oils, *Atmospheric Chemistry and Physics*, 17, 7333-7344, 10.5194/acp-17-7333-2017, 2017a.

Liu, T., Liu, Q., Li, Z., Huo, L., Chan, M., Li, X., Zhou, Z., and Chan, C. K.: Emission of volatile organic compounds and production of secondary organic aerosol from stir-frying spices, *Science of The Total Environment*, 599-600, 1614-1621, 10.1016/j.scitotenv.2017.05.147, 2017b.

Liu, T., Wang, Z., Huang, D. D., Wang, X., and Chan, C. K.: Significant Production of Secondary Organic Aerosol from Emissions of Heated Cooking Oils, *Environmental Science & Technology Letters*, 5, 32-37, 10.1021/acs.estlett.7b00530, 2017c.

Liu, T., Wang, Z., Wang, X., and Chan, C. K.: Primary and secondary organic aerosol from heated cooking oil emissions, *Atmospheric Chemistry and Physics*, 18, 11363-11374, 10.5194/acp-18-11363-2018, 2018.

Liu, T., Zhou, L., Liu, Q., Lee, B. P., Yao, D., Lu, H., Lyu, X., Guo, H., and Chan, C. K.: Secondary Organic Aerosol Formation from Urban Roadside Air in Hong Kong, *Environmental science & technology*, 53, 3001-3009, 10.1021/acs.est.8b06587, 2019.

Mao, J., Ren, X., Brune, W. H., Olson, J. R., Crawford, J. H., Fried, A., Huey, L. G., Cohen, R. C., Heikes, B., Singh, H. B., Blake, D. R., Sachse, G. W., Diskin, G. S., Hall, S. R., and Shetter, R. E.: Airborne measurement of OH reactivity during INTEX-B, *Atmospheric Chemistry And Physics*, 9, 163-173, 10.5194/acp-9-163-2009, 2009.

Masuda, M., Wang, Q., Tokumura, M., Miyake, Y., and Amagai, T.: Risk assessment of polycyclic aromatic hydrocarbons and their chlorinated derivatives produced during cooking and released in exhaust gas, *Ecotoxicology and environmental safety*, 197, 110592, 10.1016/j.ecoenv.2020.110592, 2020.

Matsui, H., Koike, M., Takegawa, N., Kondo, Y., Griffin, R. J., Miyazaki, Y., Yokouchi, Y., and Ohara, T.: Secondary organic aerosol formation in urban air: Temporal variations and possible contributions from unidentified hydrocarbons, *Journal of Geophysical Research*, 114, 10.1029/2008jd010164, 2009.

Mohr, C., DeCarlo, P. F., Heringa, M. F., Chirico, R., Slowik, J. G., Richter, R., Reche, C., Alastuey, A., Querol, X., Seco, R.,

Penuelas, J., Jimenez, J. L., Crippa, M., Zimmermann, R., Baltensperger, U., and Prevot, A. S. H.: Identification and quantification of organic aerosol from cooking and other sources in Barcelona using aerosol mass spectrometer data, *Atmospheric Chemistry And Physics*, 12, 1649-1665, 10.5194/acp-12-1649-2012, 2012.

Nash, D. G., Baer, T., and Johnston, M. V.: Aerosol mass spectrometry: An introductory review, *International Journal of Mass Spectrometry*, 258, 2-12, 10.1016/j.ijms.2006.09.017, 2006.

Ng, N. L., Canagaratna, M. R., Zhang, Q., Jimenez, J. L., Tian, J., Ulbrich, I. M., Kroll, J. H., Docherty, K. S., Chhabra, P. S., Bahreini, R., Murphy, S. M., Seinfeld, J. H., Hildebrandt, L., Donahue, N. M., DeCarlo, P. F., Lanz, V. A., Prévôt, A. S. H., Dinar, E., Rudich, Y., and Worsnop, D. R.: Organic aerosol components observed in Northern Hemispheric datasets from Aerosol Mass Spectrometry, *Atmospheric Chemistry and Physics*, 10, 4625-4641, 10.5194/acp-10-4625-2010, 2010.

Ng, N. L., Canagaratna, M. R., Jimenez, J. L., Zhang, Q., Ulbrich, I. M., and Worsnop, D. R.: Real-Time Methods for Estimating Organic Component Mass Concentrations from Aerosol Mass Spectrometer Data, *Environmental science & technology*, 45, 910-916, 10.1021/es102951k, 2011.

Nordin, E. Z., Eriksson, A. C., Roldin, P., Nilsson, P. T., Carlsson, J. E., Kajos, M. K., Hellen, H., Wittbom, C., Rissler, J., Lönndahl, J., Swietlicki, E., Svenningsson, B., Bohgard, M., Kulmala, M., Hallquist, M., and Pagels, J. H.: Secondary organic aerosol formation from idling gasoline passenger vehicle emissions investigated in a smog chamber, *Atmospheric Chemistry And Physics*, 13, 6101-6116, 10.5194/acp-13-6101-2013, 2013.

Peng, Z., Day, D. A., Ortega, A. M., Palm, B. B., Hu, W., Stark, H., Li, R., Tsigaridis, K., Brune, W. H., and Jimenez, J. L.: Non-OH chemistry in oxidation flow reactors for the study of atmospheric chemistry systematically examined by modeling, *Atmospheric Chemistry and Physics*, 16, 4283-4305, 10.5194/acp-16-4283-2016, 2016.

Presto, A. A., Gordon, T. D., and Robinson, A. L.: Primary to secondary organic aerosol: evolution of organic emissions from mobile combustion sources, *Atmospheric Chemistry and Physics*, 14, 5015-5036, 10.5194/acp-14-5015-2014, 2014.

Qin, Y. M., Tan, H. B., Li, Y. J., Schurman, M. I., Li, F., Canonaco, F., Prevot, A. S. H., and Chan, C. K.: Impacts of traffic emissions on atmospheric particulate nitrate and organics at a downwind site on the periphery of Guangzhou, China, *Atmospheric Chemistry And Physics*, 17, 10245-10258, 10.5194/acp-17-10245-2017, 2017.

Rogge, W. F., Hildemann, L. M., Mazurek, M. A., Cass, G. R., and Simonelt, B. R. T.: SOURCES OF FINE ORGANIC AEROSOL .1. CHARBROILERS AND MEAT COOKING OPERATIONS, *Environmental science & technology*, 25, 1112-1125, 10.1021/es00018a015, 1991.

Rogge, W. F., Hildemann, L. M., Mazurek, M. A., Cass, G. R., and Simoneit, B. R. T.: SOURCES OF FINE ORGANIC AEROSOL .2. NONCATALYST AND CATALYST-EQUIPPED AUTOMOBILES AND HEAVY-DUTY DIESEL TRUCKS, *Environmental science & technology*, 27, 636-651, 10.1021/es00041a007, 1993.

Seow, A., Poh, W. T., Teh, M., Eng, P., Wang, Y. T., Tan, W. C., Yu, M. C., and Lee, H. P.: Fumes from meat cooking and lung cancer risk in Chinese women, *Cancer Epidemiol. Biomarkers Prev.*, 9, 1215-1221, 2000.

Suarez-Bertoa, R., Zardini, A. A., Platt, S. M., Hellebust, S., Pieber, S. M., El Haddad, I., Temime-Roussel, B., Baltensperger, U., Marchand, N., Prévôt, A. S. H., and Astorga, C.: Primary emissions and secondary organic aerosol formation from the exhaust of a flex-fuel (ethanol) vehicle, *Atmospheric Environment*, 117, 200-211, 10.1016/j.atmosenv.2015.07.006, 2015.

Sun, Y. L., Zhang, Q., Schwab, J. J., Demerjian, K. L., Chen, W. N., Bae, M. S., Hung, H. M., Högrefe, O., Frank, B., Rattigan, O. V., and Lin, Y. C.: Characterization of the sources and processes of organic and inorganic aerosols in New York city with a high-resolution time-of-flight aerosol mass spectrometer, *Atmospheric Chemistry and Physics*, 11, 1581-1602, 10.5194/acp-11-1581-2011, 2011.

Sun, Y. L., Zhang, Q., Schwab, J. J., Chen, W. N., Bae, M. S., Hung, H. M., Lin, Y. C., Ng, N. L., Jayne, J., Massoli, P., Williams, L. R., and Demerjian, K. L.: Characterization of near-highway submicron aerosols in New York City with a high-resolution aerosol mass spectrometer, *Atmospheric Chemistry And Physics*, 12, 2215-2227, 10.5194/acp-12-2215-2012, 2012.

Tang, R. Z., Wang, H., Liu, Y., and Guo, S.: Constituents of Atmospheric Semi-Volatile and Intermediate Volatility Organic Compounds and Their Contribution to Organic Aerosol, *Prog. Chem.*, 31, 180-190, 10.7536/pc180431, 2019.

Timonen, H., Karjalainen, P., Saukko, E., Saarikoski, S., Aakko-Saksa, P., Simonen, P., Murtonen, T., Dal Maso, M., Kuuluvainen, H., Bloss, M., Ahlberg, E., Svenningsson, B., Pagels, J., Brune, W. H., Keskinen, J., Worsnop, D. R., Hillamo, R., and Rönkkö, T.: Influence of fuel ethanol content on primary emissions and secondary aerosol formation potential for a modern flex-fuel gasoline vehicle, *Atmospheric Chemistry and Physics*, 17, 5311-5329, 10.5194/acp-17-5311-2017, 2017.

Tkacik, D. S., Lambe, A. T., Jathar, S., Li, X., Presto, A. A., Zhao, Y., Blake, D., Meinardi, S., Jayne, J. T., Croteau, P. L., and

Robinson, A. L.: Secondary organic aerosol formation from in-use motor vehicle emissions using a potential aerosol mass reactor, *Environmental science & technology*, 48, 11235-11242, 10.1021/es502239v, 2014.

Ulbrich, I. M., Canagaratna, M. R., Zhang, Q., Worsnop, D. R., and Jimenez, J. L.: Interpretation of organic components from Positive Matrix Factorization of aerosol mass spectrometric data, *Atmospheric Chemistry And Physics*, 9, 2891-2918, 10.5194/acp-9-2891-2009, 2009.

Vesna, O., Sax, M., Kalberer, M., Gaschen, A., and Ammann, M.: Product study of oleic acid ozonolysis as function of humidity, *Atmospheric Environment*, 43, 3662-3669, 10.1016/j.atmosenv.2009.04.047, 2009.

Volkamer, R., Jimenez, J. L., San Martini, F., Dzepina, K., Zhang, Q., Salcedo, D., Molina, L. T., Worsnop, D. R., and Molina, M. J.: Secondary organic aerosol formation from anthropogenic air pollution: Rapid and higher than expected, *Geophysical Research Letters*, 33, 10.1029/2006gl026899, 2006.

Wang, T., Xue, L., Brimblecombe, P., Lam, Y. F., Li, L., and Zhang, L.: Ozone pollution in China: A review of concentrations, meteorological influences, chemical precursors, and effects, *The Science of the total environment*, 575, 1582-1596, 10.1016/j.scitotenv.2016.10.081, 2017.

Watne, A. K., Psichoudaki, M., Ljungstrom, E., Le Breton, M., Hallquist, M., Jerksjo, M., Fallgren, H., Jutterstrom, S., and Hallquist, A. M.: Fresh and Oxidized Emissions from In-Use Transit Buses Running on Diesel, Biodiesel, and CNG, *Environmental science & technology*, 52, 7720-7728, 10.1021/acs.est.8b01394, 2018.

Wei, W., Cheng, S., Li, G., Wang, G., and Wang, H.: Characteristics of ozone and ozone precursors (VOCs and NO_x) around a petroleum refinery in Beijing, China, *Journal of Environmental Sciences*, 26, 332-342, 10.1016/s1001-0742(13)60412-x, 2014.

Wu, Y., Zhang, S., Hao, J., Liu, H., Wu, X., Hu, J., Walsh, M. P., Wallington, T. J., Zhang, K. M., and Stevanovic, S.: On-road vehicle emissions and their control in China: A review and outlook, *The Science of the total environment*, 574, 332-349, 10.1016/j.scitotenv.2016.09.040, 2017.

Xu, W., Han, T., Du, W., Wang, Q., Chen, C., Zhao, J., Zhang, Y., Li, J., Fu, P., Wang, Z., Worsnop, D. R., and Sun, Y.: Effects of Aqueous-Phase and Photochemical Processing on Secondary Organic Aerosol Formation and Evolution in Beijing, China, *Environmental science & technology*, 51, 762-770, 10.1021/acs.est.6b04498, 2017.

Yinhui, W., Rong, Z., Yanhong, Q., Jianfei, P., Mengren, L., Jianrong, L., Yusheng, W., Min, H., and Shijin, S.: The impact of fuel compositions on the particulate emissions of direct injection gasoline engine, *Fuel*, 166, 543-552, 10.1016/j.fuel.2015.11.019, 2016.

Yu, Y., Wang, H., Wang, T., Song, K., Tan, T., Wan, Z., Gao, Y., Dong, H., Chen, S., Zeng, L., Hu, M., Wang, H., Lou, S., Zhu, W., and Guo, S.: Elucidating the importance of semi-volatile organic compounds to secondary organic aerosol formation at a regional site during the EXPLORE-YRD campaign, *Atmospheric Environment*, 118043, 10.1016/j.atmosenv.2020.118043, 2020.

Zhan, J., Feng, Z., Liu, P., He, X., He, Z., Chen, T., Wang, Y., He, H., Mu, Y., and Liu, Y.: Ozone and SOA formation potential based on photochemical loss of VOCs during the Beijing summer, *Environmental pollution*, 285, 117444, 10.1016/j.envpol.2021.117444, 2021.

Zhang, Q., Worsnop, D. R., Canagaratna, M. R., and Jimenez, J. L.: Hydrocarbon-like and oxygenated organic aerosols in Pittsburgh: insights into sources and processes of organic aerosols, *Atmospheric Chemistry And Physics*, 5, 3289-3311, 10.5194/acp-5-3289-2005, 2005.

Zhang, Q., Jimenez, J. L., Canagaratna, M. R., Ulbrich, I. M., Ng, N. L., Worsnop, D. R., and Sun, Y.: Understanding atmospheric organic aerosols via factor analysis of aerosol mass spectrometry: a review, *Analytical and Bioanalytical Chemistry*, 401, 3045-3067, 10.1007/s00216-011-5355-y, 2011.

Zhang, R., Wang, G., Guo, S., Zamora, M. L., Ying, Q., Lin, Y., Wang, W., Hu, M., and Wang, Y.: Formation of urban fine particulate matter, *Chemical reviews*, 115, 3803-3855, 10.1021/acs.chemrev.5b00067, 2015.

Zhang, Y., Deng, W., Hu, Q., Wu, Z., Yang, W., Zhang, H., Wang, Z., Fang, Z., Zhu, M., Li, S., Song, W., Ding, X., and Wang, X.: Comparison between idling and cruising gasoline vehicles in primary emissions and secondary organic aerosol formation during photochemical ageing, *The Science of the total environment*, 722, 137934, 10.1016/j.scitotenv.2020.137934, 2020a.

Zhang, Z., Zhu, W., Hu, M., Wang, H., Chen, Z., Shen, R., Yu, Y., Tan, R., and Guo, S.: Secondary Organic Aerosol from Typical Chinese Domestic Cooking Emissions, *Environmental Science & Technology Letters*, 10.1021/acs.estlett.0c00754, 2020b.

Zhao, Y., Nguyen, N. T., Presto, A. A., Hennigan, C. J., May, A. A., and Robinson, A. L.: Intermediate Volatility Organic Compound Emissions from On-Road Diesel Vehicles: Chemical Composition, Emission Factors, and Estimated Secondary Organic Aerosol Production, *Environmental science & technology*, 49, 11516-11526, 10.1021/acs.est.5b02841, 2015.

Zhao, Y., Lambe, A. T., Saleh, R., Saliba, G., and Robinson, A. L.: Secondary Organic Aerosol Production from Gasoline Vehicle

Exhaust: Effects of Engine Technology, Cold Start, and Emission Certification Standard, *Environmental science & technology*, 52, 1253-1261, 10.1021/acs.est.7b05045, 2018.

Zhao, Y. L., Saleh, R., Saliba, G., Presto, A. A., Gordon, T. D., Drozd, G. T., Goldstein, A. H., Donahue, N. M., and Robinson, A. L.: Reducing secondary organic aerosol formation from gasoline vehicle exhaust, *Proceedings of the National Academy of Sciences of the United States of America*, 114, 6984-6989, 10.1073/pnas.1620911114, 2017.

Zhong, L. J., Goldberg, M. S., Gao, Y. T., and Jin, F.: Lung cancer and indoor air pollution arising from Chinese style cooking among nonsmoking women living in Shanghai, China, *Epidemiology*, 10, 488-494, 10.1097/00001648-199909000-00005, 1999.

Zhou, W., Xu, W., Kim, H., Zhang, Q., Fu, P., Worsnop, D. R., and Sun, Y.: A review of aerosol chemistry in Asia: insights from aerosol mass spectrometer measurements, *Environmental science. Processes & impacts*, 10.1039/d0em00212g, 2020.

Table 1. Descriptions of vehicle exhaust and sampling procedures.

Experiment	Revolving Speed	Torque	Sampling Time	Parallels	Particle Density	Fuel	Sampling Line Temperature
GDI 20 km/h	1500 Hz	16 N·m	60 min	3~5			
GDI 40 km/h	2000 Hz	16 N·m	70 min	3~6	1.1~1.2 g/cm ³	Gasoline (China V, similar to Euro V)	20~25°C
GDI 60 km/h	1750 Hz	32 N·m	60 min	3~5			

639 **Table 2.** Descriptions of cooking emission and sampling procedures.

Experiment	Cooking Material	Oil Temperature	Total Cooking Time	Number of Dishes	Sampling Time	Parallels	Particle Density	Fuel & Cooware	Kitchen Volume	Sampling Line Temperature
Deep-fried Meat	170 g chicken, 500 ml corn oil and a few condiments	145~155°C	66 min	5	90 min	3~8	1.11±0.02 g/cm ³			
Shallow-fried Tofu	500 g tofu, 200 ml corn oil and a few condiments	100~110°C	64 min	5	60 min	3~5	1.04±0.03 g/cm ³	Liquefied petroleum gas (LPG) & iron wok	78 m ³ (5.6 m × 4 m × 3.5 m)	20~25°C
Stir-fried Cabbage	300 g cabbage, 40 ml corn oil and a few condiments	95~105°C	47 min	5	58 min	3~5	1.16±0.03 g/cm ³			
Kung Pao Chicken	150 g chicken, 50 g ceanut, 50 g cucumber, 40 ml corn oil and a few condiments	Unmeasured ^a	40 min	5	60 min	3~5	1.07±0.02 g/cm ³			

640 ^aIt is need to stir constantly, so the oil temperature was unstable.

641

642

643

644

645

646

647

648

649 **Table 3.** The Go: PAM condition for vehicle experiment.

Experiment	O ₃ concentration (ppbV)	OH Exposure ^a ($\times 10^{10}$ molecules·cm ⁻³ ·s)	Photochemical Age (days, [OH]= 1.5×10^6 molecules·cm ⁻³)	External OH reactivity of SO ₂ during offline calibration (S ⁻¹)	External OH reactivity of VOCs during experiment (S ⁻¹)	Ratio of OH Exposure calculated by an estimator ^b to that calculated by the decay of SO ₂ ^a	Temperature & RH in Go :PAM	Basic Description of Go: PAM	Wall Loss
GDI 20 km/h	624	7.79	0.6	15.8	10.4	119%	Temp: 19~22°C RH: 44-49%	Volume: 7.9 L. Flow rate: 4 L/min for sample air and 1 L/min for sheath gas. Residence time: 110 s.	The wall loss of particle have been adjusted in each size bin measured by two synchronous SMPS (two SMPS ran before and after Go: PAM respectively).The wall loss of gas phase is minor according to previous research.
	2367	21.4	1.7						
	4433	37.4	2.9						
	6533	53.8	4.2						
	8050	65.6	5.1						
	8701	70.6	5.5						
GDI 40 km/h	The same as 20 km/h experiments				20.2	83%			
GDI 60 km/h	The same as 20 km/h experiments				16.7	94%			

^aOH exposure was calculated based on the decay of SO₂.
^bOH exposure for each ingredient was calculated based on the OFR estimator.

658 **Table 4.** The Go: PAM condition for cooking experiment.

Experiment	O ₃ concentration (ppbV)	OH Exposure ^a (×10 ¹⁰ molecules·cm ⁻³ ·s)	Photochemical Age (days, [OH]=1.5×10 ⁶ molecules·cm ⁻³)	External OH reactivity of SO ₂ during offline calibration (S ⁻¹)	External OH reactivity of VOCs during experiment (S ⁻¹)	Ratio of OH Exposure calculated by an estimator ^b to that calculated by the decay of SO ₂ ^a	Temperature & RH in Go: PAM	Basic Description of Go: PAM	Wall Loss
	-	0	0.0						
Deep-fried Chicken	310	4.3	0.3						The wall loss of particle have been adjusted in each size bin measured by two synchronous SMPS (two SMPS ran before and after Go: PAM respectively).The wall loss of gas phase is minor according to previous research.
	1183	9.6	0.7		25.7	97%			
	2217	14.4	1.1						
	3267	21.4	1.7						
	4025	27.1	2.1						
Shallow-fried Tofu	The same as Deep-fried Chicken experiments			24.0	21.7	111%	Temp: 16~19°C RH: 18~23%	Volume: 7.9 L. Flow rate: 7 L/min for sample air and 3 L/min for sheath gas. Residence time: 55 s.	
Stir-fried Cabbage	The same as Deep-fried Chicken experiments				23.3	104%			
Kung Pao Chicken	The same as Deep-fried Chicken experiments				23.6	103%			

^aOH exposure was calculated based on the decay of SO₂.
^bOH exposure for each ingredient was calculated based on the OFR estimator.

Table 5. A summary of elemental ratios and dominant peaks among various SOA.

Type	O/C	H/C	f_{28}	f_{29}	f_{41}	f_{43}	f_{44}	f_{55}	f_{57}	Dominant Peaks (In decedning order)
GDI LO-OOA	0.46	1.80	0.066	0.076	0.051	0.133	0.077	0.043	0.029	m/z 43, 44, 29, 28, 41, 55
GDI MO-OOA	0.91	1.57	0.134	0.071	0.026	0.117	0.146	0.024	0.013	m/z 44, 28, 43, 29, 45, 27
Cooking LO-OOA	0.36	1.92	0.053	0.065	0.058	0.097	0.065	0.056	0.046	m/z 43, 44, 29, 41, 55, 28
Heated oil SOA (Liu, 2018)	0.38	1.53	0.070	0.087	0.067	0.078	0.067	0.053	0.023	m/z 29, 43, 28, 44, 41, 55
Meat charbroiling SOA (Kaltsonoudis, 2017)	0.24	1.83	0.039	0.061	0.077	0.075	0.052	0.074	0.035	m/z 41, 43, 55, 29, 27, 44
Gasoline SOA (Nordin, 2013)	0.40	1.38	0.122	0.032	0.031	0.094	0.129	0.019	0.008	m/z 44, 28, 39, 27, 29, 41
Disel SOA (Chirico, 2010)	0.37	1.57	0.069	0.092	0.062	0.112	0.073	0.045	0.022	m/z 43, 29, 44, 28, 41, 27

Table 6. Pearson correlations between laboratory OA and ambient OA mass spectra.

Pearson Correlation ($\alpha=0.05$)	Ambient HOA	Ambient COA	Ambient LO-OOA	Ambient MO-OOA
Lab Cooking POA	0.95	0.86	0.46	0.39
Lab Cooking LO-OOA	0.90	0.81	0.76	0.68
Lab Vehicle LO-OOA	0.80	0.71	0.81	0.73
Lab Vehicle MO-OOA	0.54	0.44	0.98	0.94

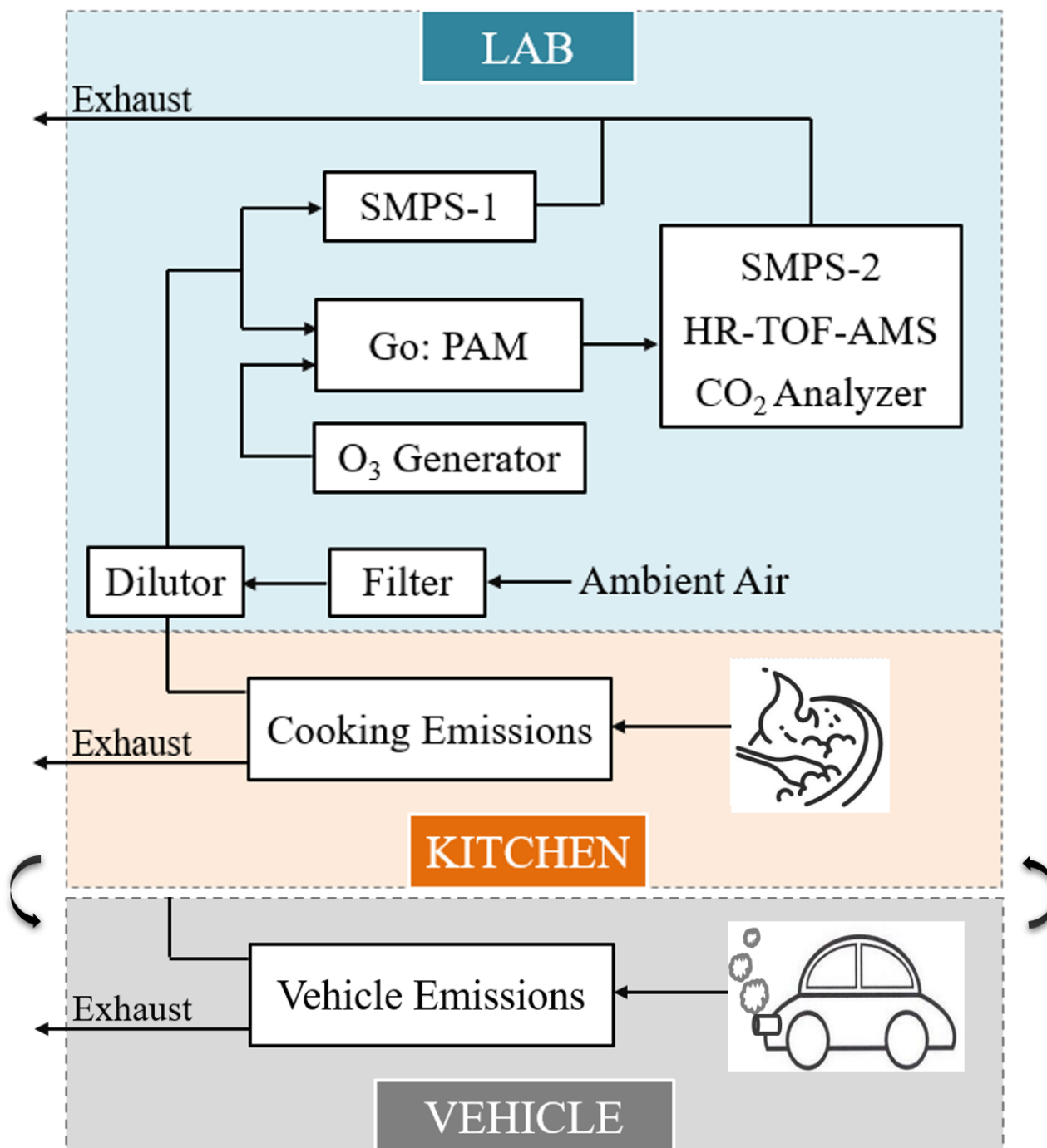


Figure 1. Schematic of experiment system.

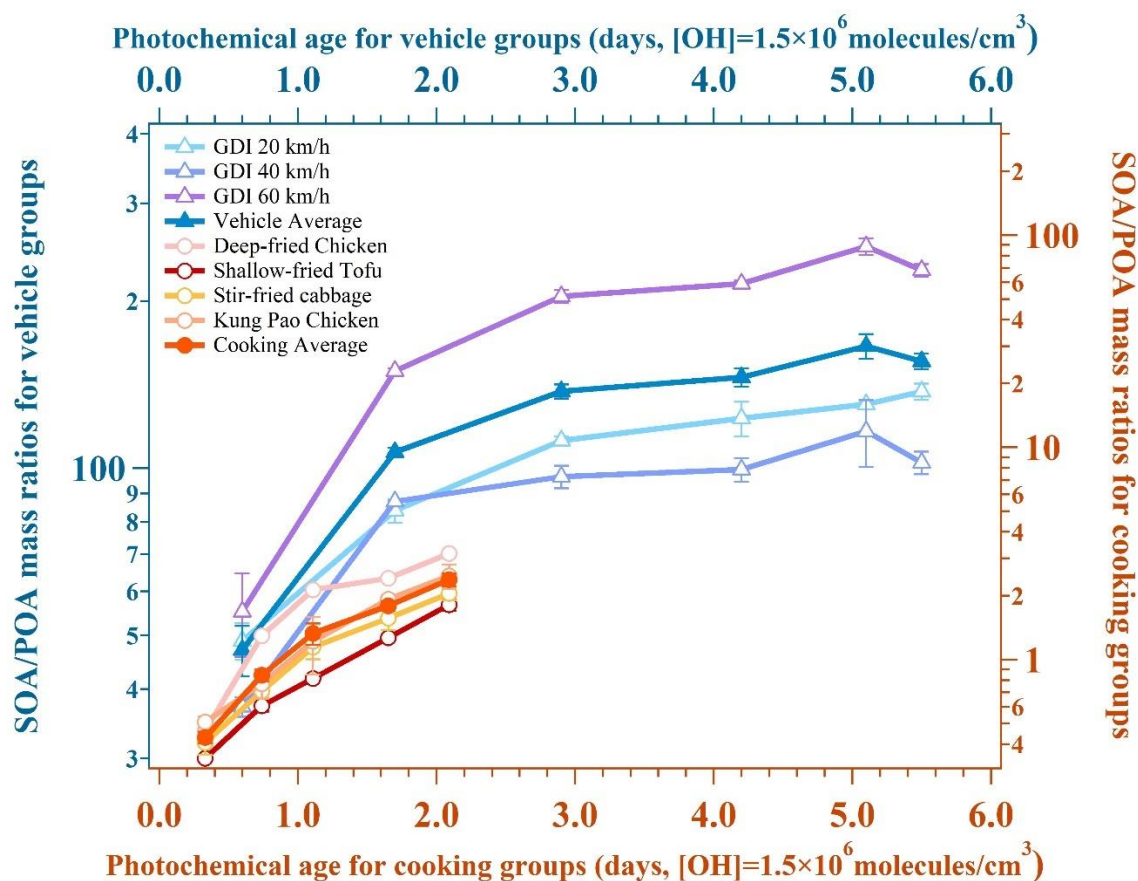


Figure 2. Secondary mass growth potentials for two urban lifestyle SOA. The SMPS-1 determined the mass concentration of POA, while the SMPS-2 determined the mass concentration of aged OA, and their mass difference could be regarded as the SOA. The average data and standard deviation bars are shown in the figure.

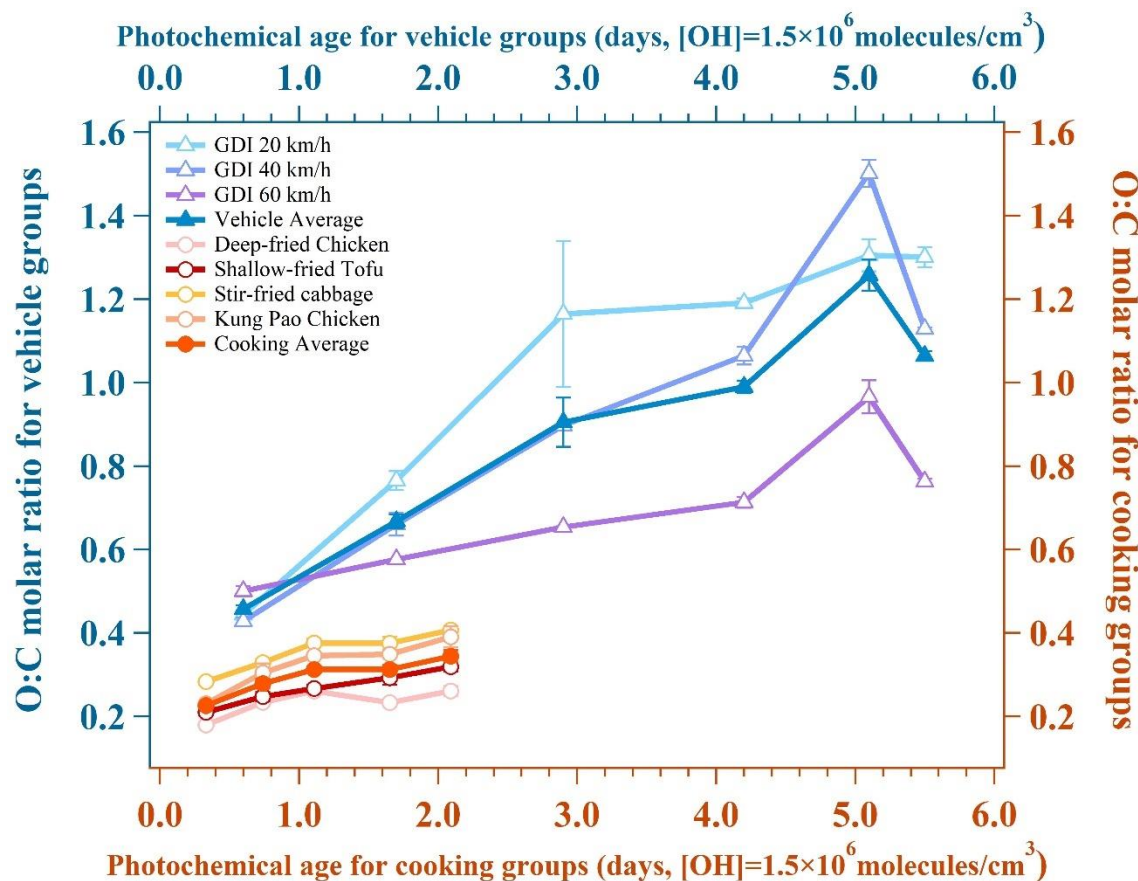


Figure 3. Evolution of O:C molar ratio for two urban lifestyle OA. The O:C molar ratios are determined by HR-Tof-AMS. The average data and standard deviation bars at each gradient are shown in the figure.

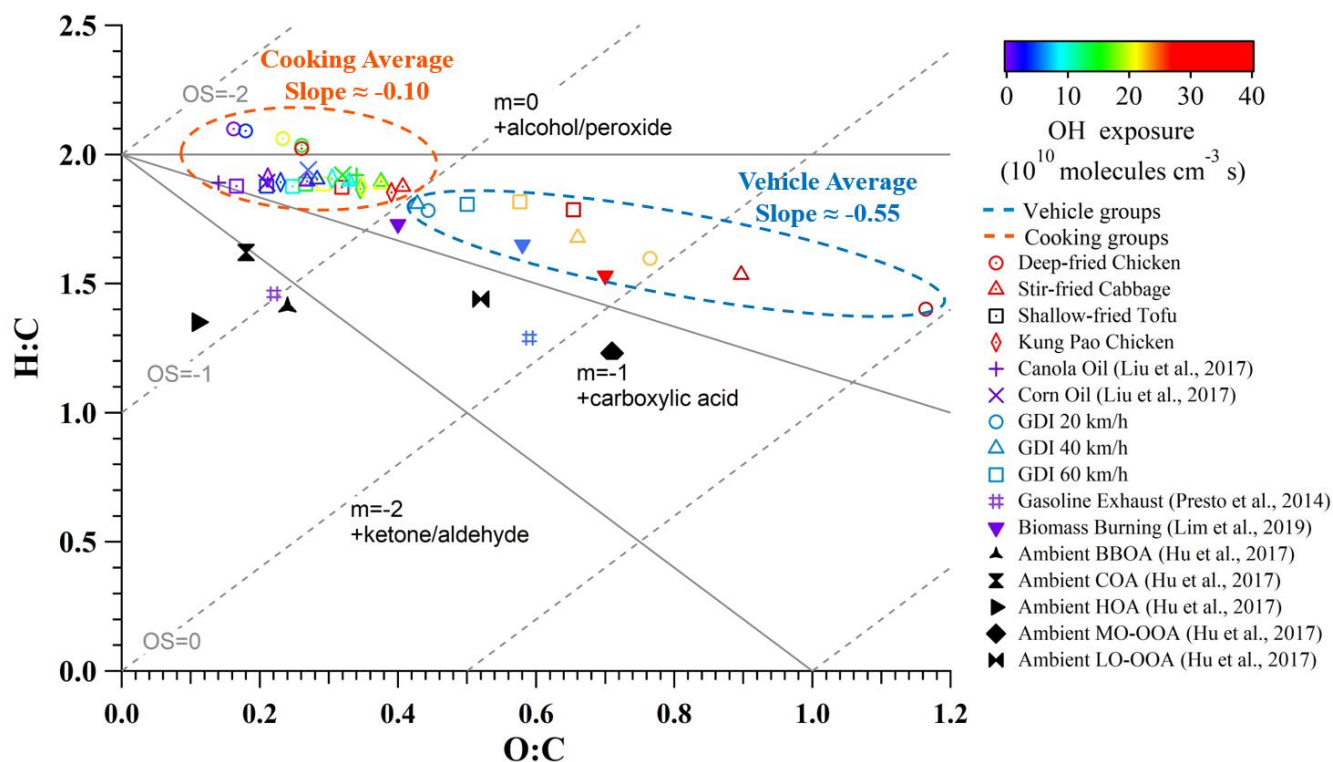


Figure 4. Van Krevelen diagram of OA from various sources. The O:C and H:C are determined by HR-ToF-AMS. The average data at each gradient are shown in the figure.

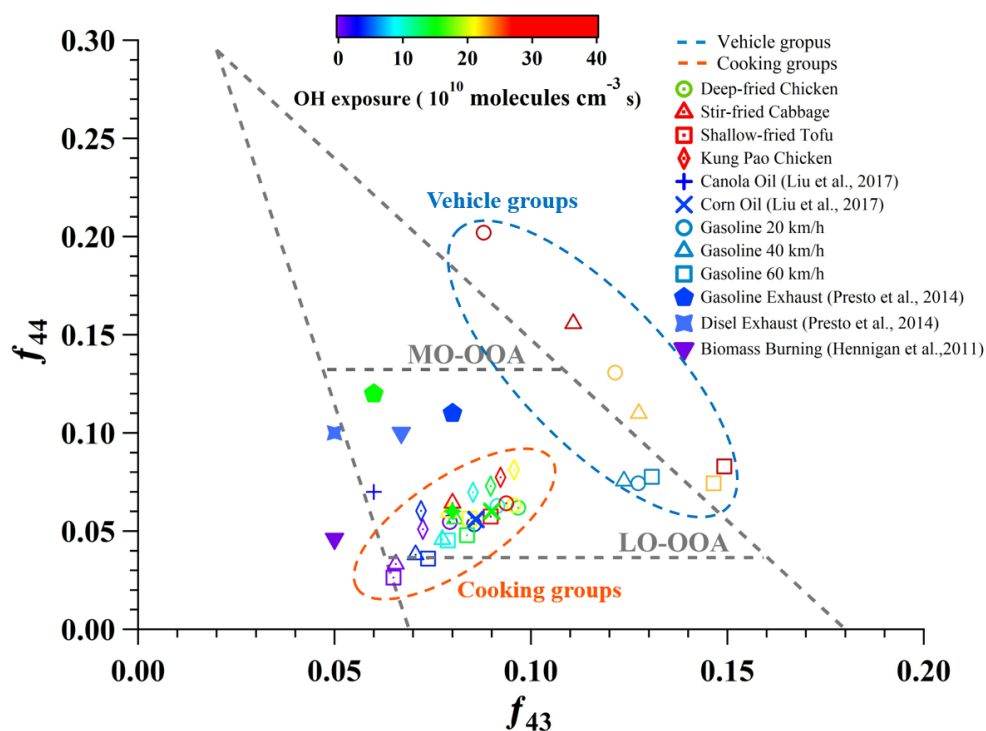


Figure 5. Fractions of entire organic signals at m/z 43 (f_{43}) vs. m/z 44 (f_{44}) from various sources as well as Ng triangle plot. The f_{43} and f_{44} are determined by HR-ToF-AMS. The average data at each gradient are shown in the figure.

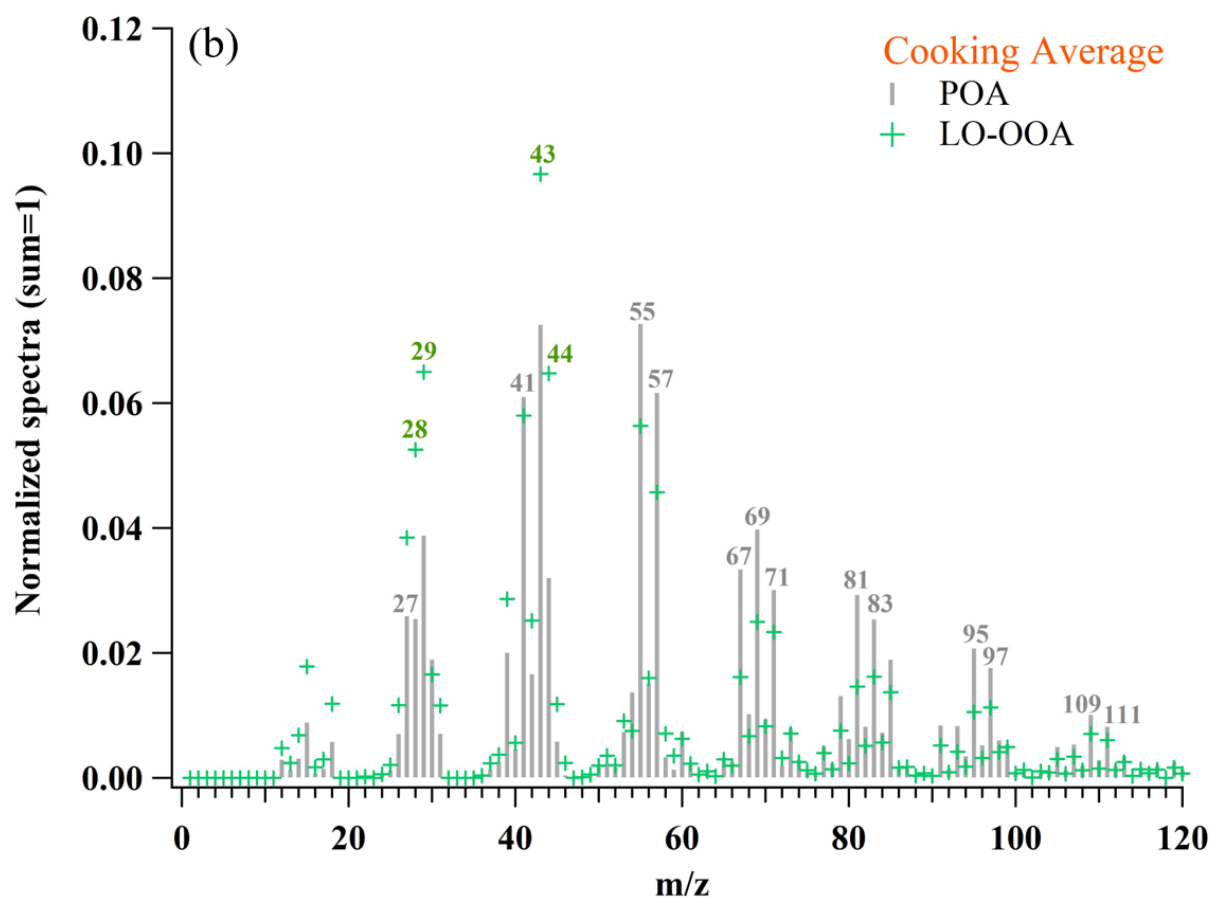
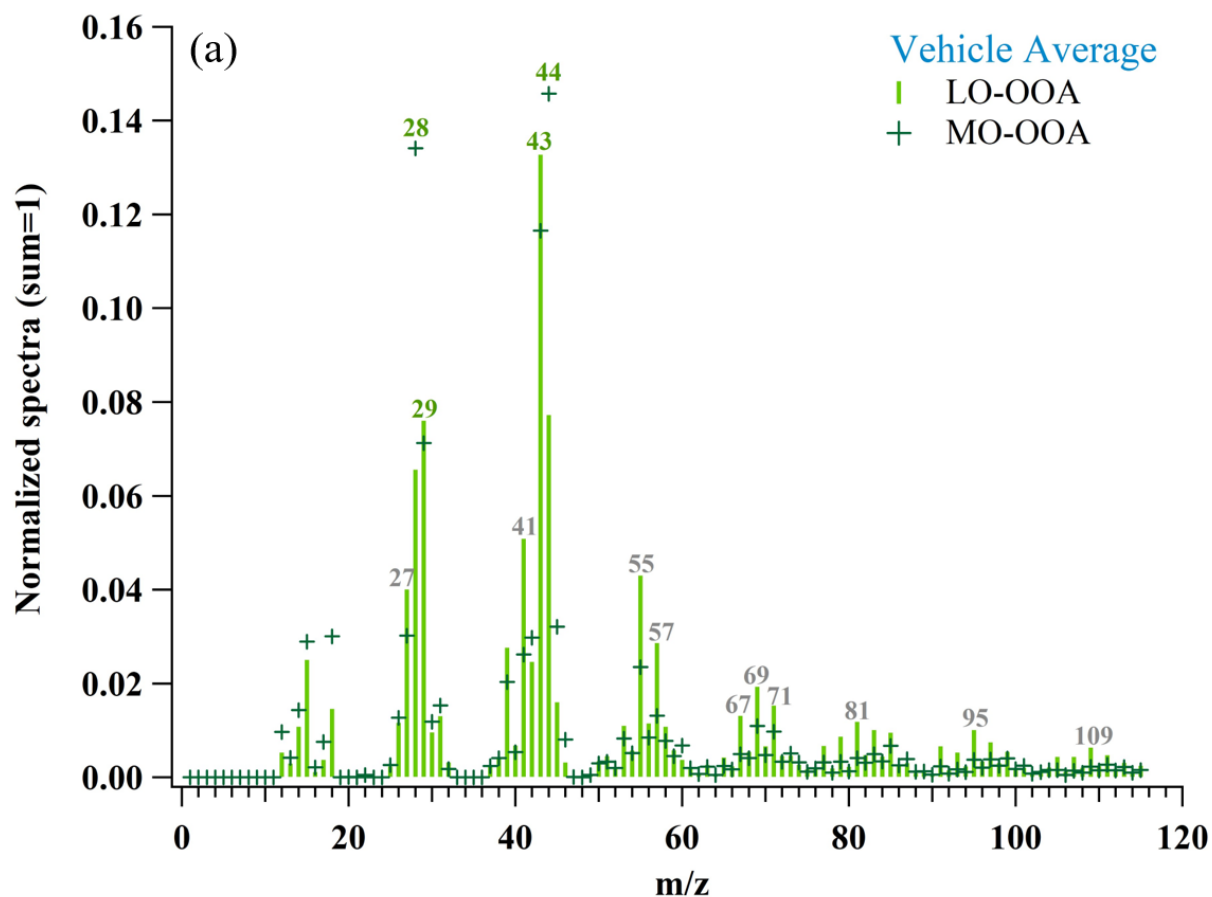


Figure 6. Average mass spectra of OA from two urban lifestyle sources. The numbered symbols represent the m/z values with relatively large fractions. The gray symbols represent the fragments that mainly come from hydrocarbon-like fragments and the green symbols represent those mainly come from oxygen-containing fragments. The mass spectra are determined by HR-ToF-AMS. The average data are shown in the figure.

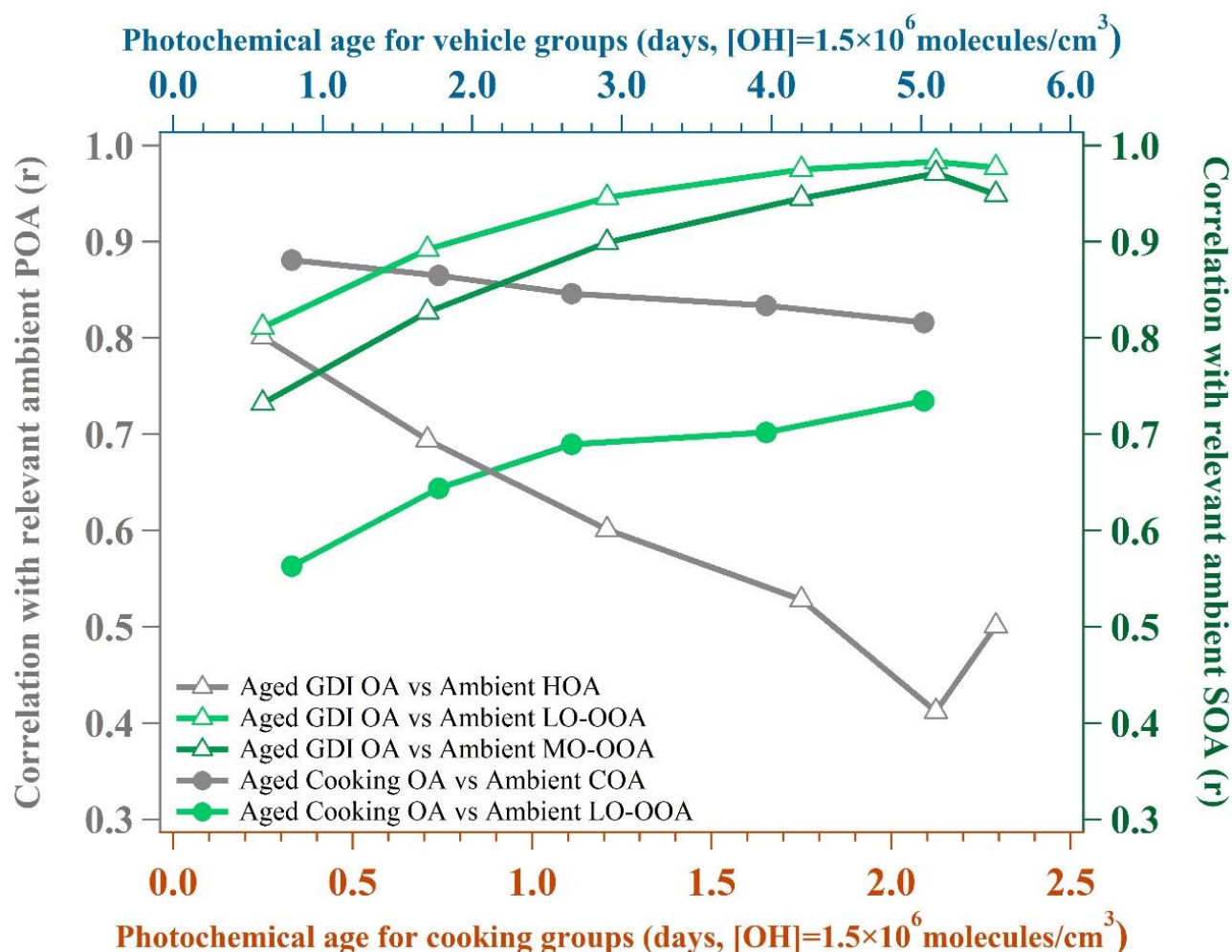


Figure 7. Correlation coefficients (Pearson r) between the laboratory aged OA and published ambient PMF-OA factors with growing photochemical ages. Ambient PMF-OA factors are the average results from two field studies in Beijing (Measured at a typical urban site during autumn and winter; Autumn: Oct. 1st, 2018 – Nov. 15th, 2018; Winter: Jan. 5th, 2019 – Jan. 31st, 2019). The unit mass resolution mass spectra are determined by HR-ToF-AMS.

Supplement of

Formation and Evolution of Secondary Organic Aerosol Derived from Urban Lifestyle Sources: Vehicle Exhaust and Cooking Emission

Zirui Zhang^{§,1}, Wenfei Zhu^{§,1}, Min Hu^{*,1,2,5}, Kefan Liu¹, Hui Wang¹, Rongzhi Tang¹, Ruizhe Shen¹, Ying Yu¹, Rui Tan¹, Kai Song¹, Yuanju Li¹, Wenbin Zhang³, Zhou Zhang³, Hongming Xu³, Shijin Shuai³, Shuangde Li⁴, Yunfa Chen⁴, Jiayun Li⁶, Yuesi Wang⁶, Song Guo¹

¹State Key Joint Laboratory of Environmental Simulation and Pollution Control, International Joint Laboratory for Regional Pollution Control, Ministry of Education (IJRC), College of Environmental Sciences and Engineering, Peking University, Beijing 100871, China

²Collaborative Innovation Center of Atmospheric Environment and Equipment Technology, Nanjing University of Information Science & Technology, Nanjing 210044, China

³State Key Laboratory of Automotive Safety and Energy, Tsinghua University, Beijing 100084, China

⁴State Key Laboratory of Multiphase Complex Systems, Institute of Process Engineering, Chinese Academy of Sciences, Beijing 100190, China

⁵Beijing Innovation Center for Engineering Sciences and Advanced Technology, Peking University, Beijing 100871, China

⁶State Key Laboratory of Atmospheric Boundary Layer Physics and Atmospheric Chemistry (LAPC), Institute of Atmospheric Physics, Chinese Academy of Sciences, Beijing 100029, China

[§]These authors contributed equally to this work.

Corresponding authors:

*Min Hu – State Key Joint Laboratory of Environmental Simulation and Pollution Control, College of Environmental Sciences and Engineering, Peking University, Beijing 100871, China; Email: minhu@pku.edu.cn

List of the supporting information:

Section S1. Details about vehicle and cooking laboratory experiments

Section S2. Go: PAM conditions

Table S1. Comparison of results between blank and experimental groups (Dilution air and boiled water are two kinds of blank groups. The others are experimental groups).

Table S2. Test engine information.

Table S3. Catalyst system information.

Table S4. The comparison of SOA/POA between SMPS and AMS-PMF results. “SOA/POA (SMPS)” means the mass ratio gained from SMPS-1 and SMPS-2. “SOA/POA (AMS-PMF)” means the mass ratio gained from PMF analysis of aged OA measured by HR-ToF-AMS.

Table S5. VOCs measured by GC-MS at the inlet of Go: PAM.

Table S6. K_{OH} of major species in Go: PAM.

Table S7. Comparison of primary (no O_3 , UV OFF), O_3 oxidation (certain O_3 , UV OFF), and OH oxidation (certain O_3 , UV ON) results during the cooking experiment.

Figure S1. Profile of Go: PAM.

Figure S2. Comparison of measured and estimated OH exposures during off-line OH exposure calibration of the vehicle experiment.

Figure S3. Comparison of measured and estimated OH exposures during off-line OH exposure calibration of the cooking experiment.

Figure S4. Previous performance tests for Go: PAM.

Figures S5-S8. Mass spectra of PMF-resolved POA and SOA factors for the cooking experiment.

Figures S9-S12. Diagnostic plots of the PMF analysis for the cooking experiment.

Section S1: Details about vehicle and cooking laboratory experiments.

The vehicle experiment was conducted from July to October in 2019, at the Department of Automotive Engineering, Tsinghua University. For all experiments, the gasoline direct injection (GDI) engine ran in a single room, its exhaust was drawn into the pipeline and then entered the Go: PAM at a 30 fold dilution where aerosols and gases reacted at a stable temperature and relative humidity. The GDI engine was equipped with a three-way catalyst system, and its parameters are shown in Table S2-S3. The cooking experiment was conducted from November 2019 to January 2020, at Langfang Branch, Institute of Process Engineering, Chinese Academy of Sciences. The cooking time and oil temperature were different due to the inherent features of the ingredients. For all experiments, the closed kitchen was full of fumes where the vision was blurred and the air was choky after a long time of the cooking process. Subsequently, the cooking fumes were drawn into pipeline from a kitchen to a lab and then entered the Go: PAM at an 8 fold dilution where aerosols and gases reacted at a stable temperature and relative humidity. From the sampling port at the source (cooking and vehicle) to the inlet of HR-ToF-AMS, the 3/8 inch (inner diameter was 6 mm) stainless steel tubes were totally 7 meters long and the corresponding residence time was 4.9s. There were 5 meters long from the sampling port to the Go: PAM, and the flow rate was 5.5 L/min (HR-ToF-AMS and other instruments jointly determined the flow rate). There were 2 meters long from the Go: PAM to the HR-ToF-AMS, and the flow rate was 1 L/min (HR-ToF-AMS and its drainage system determined the flow rate).

The dilution air was ambient air (clean period), which was firstly filtered by a particle filter system (including a dryer, a filter, and an ultrafilter, SMC Inc.) in order to remove the particles and water. Then the dilution air was filtered by an activated carbon adsorption device, in order to remove the VOCs. The vehicle exhaust from the tailpipe was first diluted by a gradient heated dilution system (6 fold) and then diluted by an unheated dilution system (5 fold). The temperature of sample flow was near indoor temperature after secondary dilution systems. The cooking fumes were collected through the kitchen ventilator. The boiled water can be a background sample influenced by indoor air, iron wok, and ventilator. As the results of blank groups in Table S1 show, the dilution air and background interference just made a minor influence on the SOA concentration.

Besides, a temperature controller and heat insulation cotton were wrapped around the sampling pipelines to prevent freshly warm gas from condensing on the pipe wall. Silicon tubes were used to dry the emissions before they entered measuring instruments. The particle densities were measured through the determination of the DMA-CPMA-CPC system (DMA- Differential Mobility Analyzer; CPMA- Centrifugal Particle Mass Analyzer; CPC- Condensation Particle Counter) in our study. Prior to each experiment, all pipelines and the Go: PAM chamber were continuously flushed with purified dry air until the concentrations of gases and particles were minimal. Furthermore, blank experiments were separately designed in the presence of boiling water emissions or dilution air under the same condition. The results of blank groups can be found in Table S1. When the OH exposure was zero, OA concentrations derived from dilution air were so low that they couldn't be quantified correctly. On the whole, the OA concentrations of blank groups were far below those of experimental groups. The field study was deployed at the Institute of Atmospheric Physics (IAP), Chinese Academy of Sciences (39°58'N; 116°22'E) in autumn and winter (Autumn: Oct. 1st, 2018 – Nov. 15th, 2018; Winter: Jan. 5th, 2019 – Jan. 31st, 2019) (Li et al., 2020a).

The sample site is located in the south of Beitucheng West Road and west of Beijing Chengde expressway in Beijing, which is a typical urban site affected by local emissions (Li et al., 2020b).

Section S2: Go: PAM conditions

As Figure S1 shows, the flow reactor of Go: PAM is made of quartz glass (1) (Raesh GmbH RQ 200), which is 100 cm long and 9.6 cm in diameter. About 84 cm of the flow reactor may be illuminated by either one or two Philips TUV 30 W fluorescent tubes (2), each radiating about 10 W at 254 nm. It is enclosed in a compartment of aluminum mirrors, in order to reduce the inhomogeneity of the photon field inside the reactor. The fluorescent tubes and quartz tubes are surrounded by a parabolic trough mirror (3), 90 deg. flat mirror (4) and 45-90 deg. flat mirrors (5). The shell of Go: PAM is composed of a sheath metal cover (6) and square tubing support structure (7) (Watne et al., 2018). As for the vehicle and cooking experiment, the photon flux at 254 nm was 4.5×10^{14} and 2.2×10^{15} photons·cm⁻²·s⁻¹, respectively.

Table S7 shows the comparison of primary (no O₃, UV OFF), O₃ oxidation (certain O₃, UV OFF) and OH oxidation (certain O₃, UV ON) results during the cooking experiment. There is no significant increase in OA mass when we just add O₃ with UV off, comparing to those of OH oxidation groups (input O₃ with UV on). Overall, our Go: PAM could reasonably simulate the OH oxidation process of cooking OA in ambient. The detailed information of gaseous compounds and their K_{OH} can be found in Table S5-S6. The K_{OH} for each specie was taken from the updated Carter research results (<http://www.engr.ucr.edu/~carter/reactdat.htm>, last access: 24 February 2021).

The mixing and wall loss tests have already conducted in previous work using the same Go: PAM according to Li et al. (Li et al., 2019) and Watne et al. (Watne et al., 2018). In Figure S3(a), SO₂ was continually injected into the “4 Humidified oxidant flow” and “5 Sample flow”, and was measured through “3 Processed sample flow” (Watne et al., 2018). As shown in Figure S3(b), there was nearly no difference when using different inlets, which demonstrated a great mixing of the sample and oxidant flow in the Go: PAM (Watne et al., 2018). Figure S3(c) modeled the wall loss of LVOC (low-volatility VOC) following the method of Palm et al. (Watne et al., 2018; Palm et al., 2016). The results indicated that most LVOC tended to react with OH or condensate on particles rather than exit or cause loss to the wall (Li et al., 2019). Figure S3(d) tested the particle wall loss using nebulized ammonium sulfate particles. Results showed that the particle losses with size above 22.1 nm were nearly smaller than 10% which would only make a negligible effect in Go: PAM (Watne et al., 2018), while in this study, we still corrected the wall loss of particle in each size bin measured by two synchronous SMPS (two SMPS run before and after Go: PAM respectively).

Table S1. Comparison of results between blank and experimental groups (Dilution air and boiled water are two kinds of blank groups. The others are experimental groups).

Experiment	OH Exposure ($\times 10^{10}$ molecules·cm ⁻³ ·s)	OA Concentration (μg/m ³)	Standard Deviation	Relative Standard Deviation
Dilution Air (cooking)	0	-	-	-
	9.6	0.37	0.04	12%
Boiled Water	0	0.04	0.02	44%
	9.6	0.36	0.12	32%
Deep-fried Chicken	0	12.30	0.49	4%
	9.6	28.29	2.55	9%
Shallow-fried Tofu	0	13.56	0.68	5%
	9.6	21.70	1.08	5%
Stir-fried Cabbage	0	10.75	0.65	6%
	9.6	18.38	1.65	9%
Kung Pao Chicken	0	6.47	0.52	8%
	9.6	11.39	1.25	11%
Dilution Air (vehicle)	0	-	-	-
	7.8	0.52	0.07	13%
GDI 20 km/h	0	0.40	0.01	3%
	7.8	19.68	1.48	8%
GDI 40 km/h	0	0.41	0.01	3%
	7.8	15.24	0.62	4%
GDI 60 km/h	0	0.42	0.02	5%
	7.8	23.23	4.00	17%

Table S2. Test engine information.

Specification	GDI
Displaced Volume	998 cc
Stroke	78.6 mm
Bore	73.4 mm
Compression ratio	9.6
Max power / engine speed	100 kW / 6000 rpm
Max torque / engine speed	205 N·m / 2000-3000 rpm

Table S3. Catalyst system information.

Specification	Three-way catalyst system
Volume	1.19 L
Material	Cordierite
Diameter	132.1 mm
Length	87.1 mm
Cell	900 /inch ²

Table S4. The comparison of SOA/POA between SMPS and AMS-PMF results. “SOA/POA (SMPS)” means the mass ratio gained from SMPS-1 and SMPS-2. “SOA/POA (AMS-PMF)” means the mass ratio gained from PMF analysis of aged OA measured by HR-ToF-AMS.

Photochemical Age (days, [OH]= 1.5×10^6 molecules·cm ⁻³)	Deep Fried Chicken		Shallow-fried Tofu		Stir-fried cabbage		Kung Pao Chicken		Cooking Average	
	SOA/POA (AMS-PMF)	SOA/POA (SMPS)	SOA/POA (AMS-PMF)	SOA/POA (SMPS)	SOA/POA (AMS-PMF)	SOA/POA (SMPS)	SOA/POA (AMS-PMF)	SOA/POA (SMPS)	SOA/POA (AMS-PMF)	SOA/POA (SMPS)
0.3	0.63	0.46	0.34	0.34	0.50	0.41	0.53	0.51	0.50	0.43
0.7	1.84	1.29	1.29	0.61	0.93	0.71	0.87	0.77	1.23	0.84
1.1	2.21	2.13	1.97	0.81	1.87	1.14	1.44	1.22	1.87	1.33
1.7	2.30	2.41	3.32	1.27	1.95	1.57	4.57	1.92	3.03	1.79
2.1	3.23	3.16	4.50	1.81	2.04	2.05	6.28	2.48	4.01	2.38

Table S5. VOCs measured by GC-MS at the inlet of Go: PAM.

Expriment	TVOCs (ppbV)	Alkane (%)	Alkene (%)	Aromatic (%)	O-VOC (%)	X-VOC (%)
GDI 20 km/h	33	60%	6%	12%	13%	9%
GDI 40 km/h	35	55%	7%	13%	13%	12%
GDI 60 km/h	29	54%	6%	12%	14%	13%
Deep-fried Chicken	139	21%	7%	6%	29%	37%
Shallow-fried Tofu	124	57%	9%	10%	18%	7%
Stir-fried Cabbage	127	48%	8%	14%	21%	10%
Kung Pao Chicken	189	64%	8%	11%	5%	13%

Table S6. K_{OH} of major species in Go: PAM.

Species	$K_{OH} (cm^{-3} \cdot molecules^{-1} \cdot s^{-1})$
Alkanes	
Ethane	2.48E-13
iso-Pentane	3.59E-12
Propane	1.09E-12
n-Butane	2.36E-12
iso-Butane	2.12E-12
n-Pentane	3.79E-12
2,3-Dimethylbutane	5.77E-12
3-Methylpentane	5.19E-12
n-Hexane	5.19E-12
n-Butane	2.36E-12
1,2-Dichloroethane	2.39E-13
2,3-Dimethylpentane	1.50E-12
3-Methylpentane	5.19E-12
Methylcyclopentane	8.60E-12
2-Methylpentane	5.19E-12
2-Methylheptane	7.00E-12
n-Heptane	6.76E-12
Alkenes	
Ethylene	8.52E-12
Isoprene	1.00E-10
Propene	2.62E-11
trans-2-Pentene	6.69E-11
Aromatics	
m/p-Xylene	1.87E-11
Toluene	5.63E-12
1,2,4-Trimethylbenzene	3.25E-11
o-Xylene	1.36E-11
Benzene	1.22E-12
m/p-Xylene	1.87E-11
O-VOCs	
Acetaldehyde	1.50E-11
Acetone	1.70E-13
MTBE	2.93E-12
MethylEthylKetone	1.22E-12
MethylVinylKetone	2.00E-11
n-Hexanal	2.99E-11
Acrolein	2.00E-11
n-Pentanal	2.79E-11
X-VOCs	
Tetrachloroethylene	1.59E-13
MethyleneChloride	1.48E-13
Freon	0.00E+00
Chloroform	1.03E-13
Chloromethane	4.30E-14
Inorganic	
SO ₂	9.00E-13
NO _x	1.00E-11

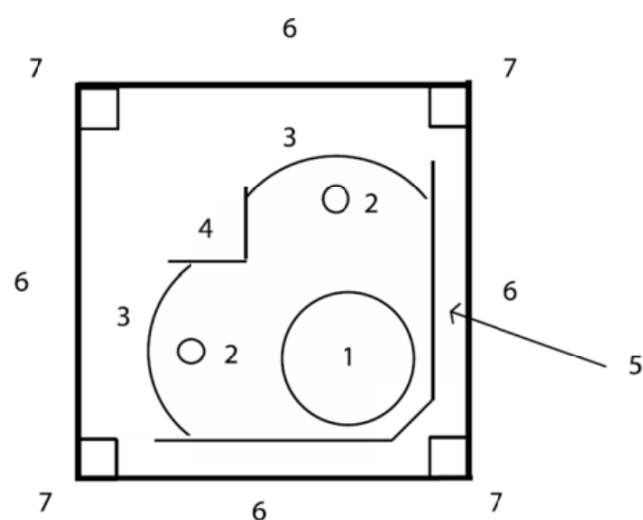
Table S7. Comparison of primary (no O₃, UV OFF), O₃ oxidation (certain O₃, UV OFF) and OH oxidation (certain O₃, UV

144 ON) results during the cooking experiment.

Experiment	Input O ₃ concentration (ppbV)	UV	OH Exposure ($\times 10^{10}$ molecules·cm ⁻³ ·s)	OA Concentration (μg/m3)	Standard Deviation	Relative Standard Deviation
Dilution Air (cooking)	-	OFF	0	-	-	-
	-	ON	9.6	0.37	0.04	12%
Boiled Water	-	OFF	0	0.04	0.02	44%
	-	ON	9.6	0.36	0.12	32%
Deep-fried Chicken	-	OFF	0	12.30	0.49	4%
	1183	OFF	-	14.50	0.20	1%
	1183	ON	9.6	28.29	2.55	9%
Shallow-fried Tofu	-	OFF	0	13.56	0.68	5%
	1183	OFF	-	14.79	3.25	22%
	1183	ON	9.6	21.70	1.08	5%
Stir-fried Cabbage	-	OFF	0	10.75	0.65	6%
	1183	OFF	-	12.70	0.72	6%
	1183	ON	9.6	18.38	1.65	9%
Kung Pao Chicken	-	OFF	0	6.47	0.52	8%
	1183	OFF	-	/	/	/
	1183	ON	9.6	11.39	1.25	11%

145

146



147

148 **Figure S1.** Profile of Go: PAM. (1) 9.6 cm quartz tube (2) fluorescent tube (3) parabolic trough mirror (4)90 deg. flat
149 mirror (5) 45-90 deg. flat mirror (6) sheath metal cover (7) Square tubing support structure (Watne et al., 2018).

150

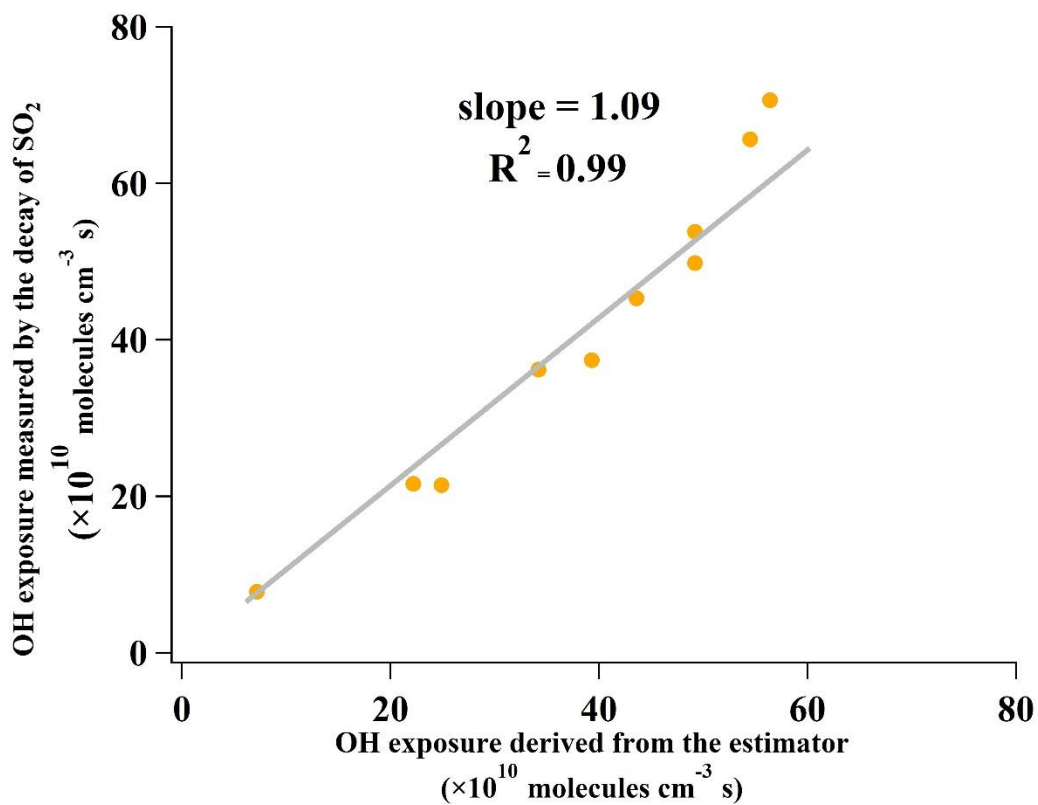


Figure S2. Comparison of measured and estimated OH exposures during off-line OH exposure calibration of the vehicle experiment.

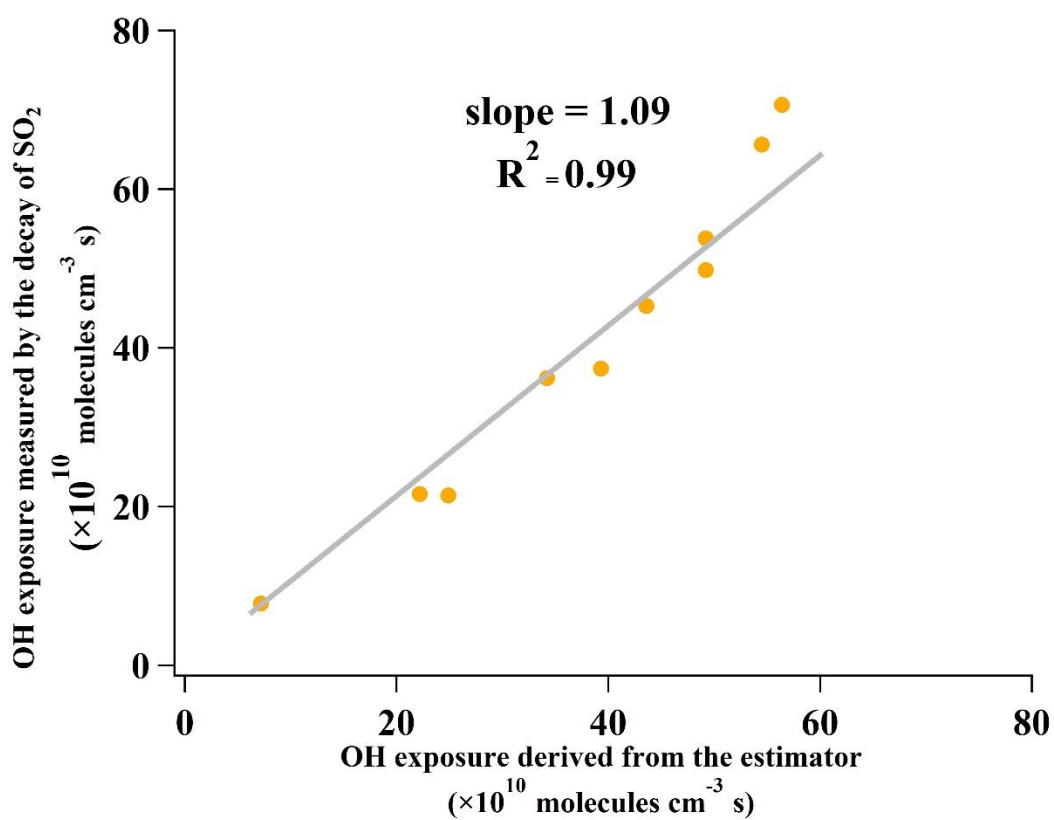


Figure S3. Comparison of measured and estimated OH exposures during off-line OH exposure calibration of the cooking experiment.

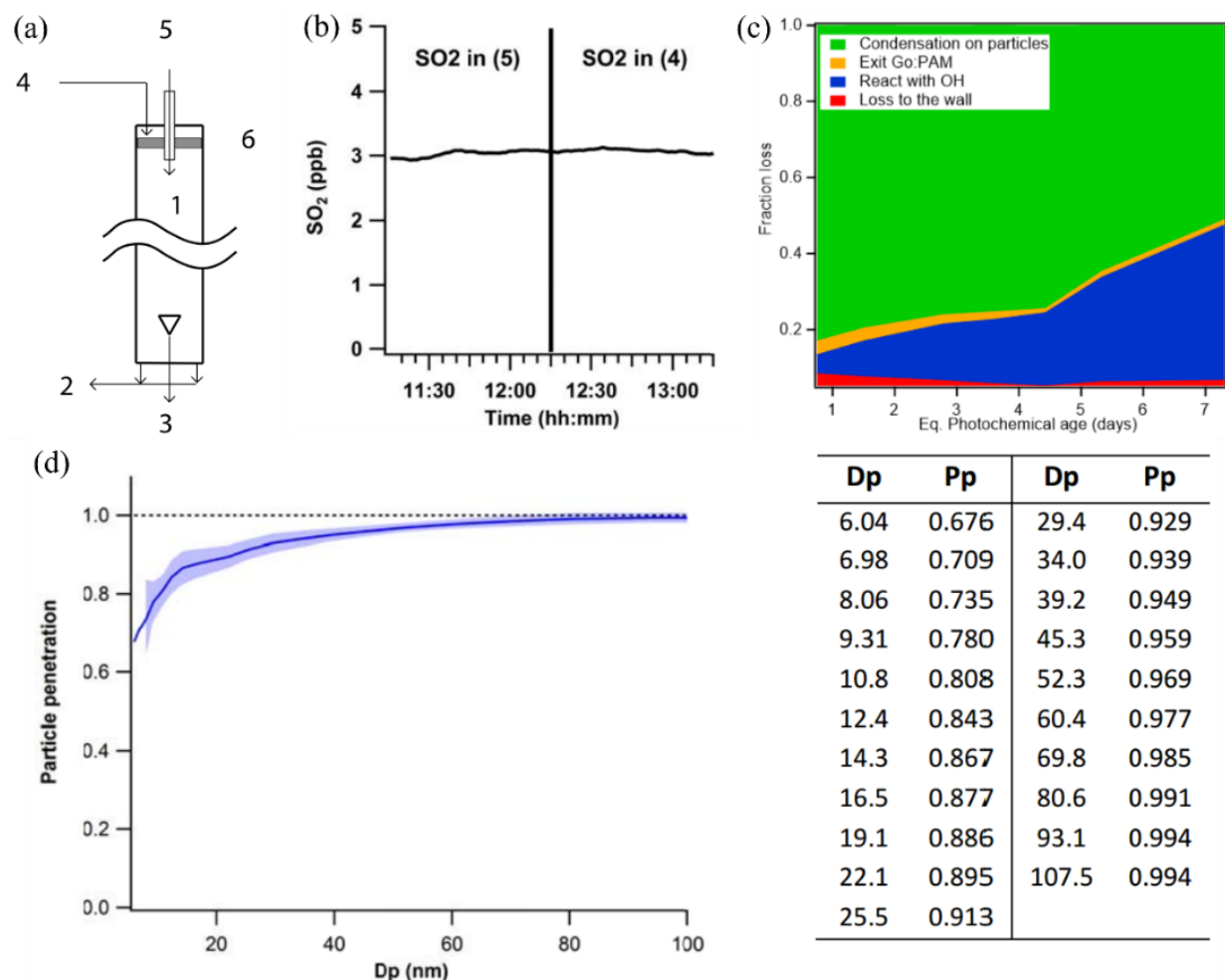


Figure S4. Previous performance tests for Go: PAM: (a) The schematic diagram of the Go: PAM reactor. (1) Quartz glass flow reactor; (2) Exhaust flow; (3) Processed sample flow; (4) Humidified oxidant flow; (5) Sample flow; (6) Gas distributor plate (Watne et al., 2018). (b) SO_2 added in turn in the “sample flow” (flow 5) and the “oxidant flow” (flow 4), and sampled from “processed sample flow” (Watne et al., 2018). (c) Modeled fractional fates of LVOCs loss as a function of the equivalent photochemical age in the Go: PAM (Li et al., 2019). (d) The particle penetration (Pp) as a function of the particle mobility diameter (Dp) in Go: PAM. The solid line and shaded area represent the average and one standard deviation of the five different mass loadings of the nebulized ammonium sulfate particles (39–258 $\mu\text{g}/\text{m}^3$), respectively. The dashed black line represents 100% of particle penetration. The values for the first two size bins (6.04 and 6.98 nm) were extrapolated due to the low signal-to-noise ratio (Watne et al., 2018).

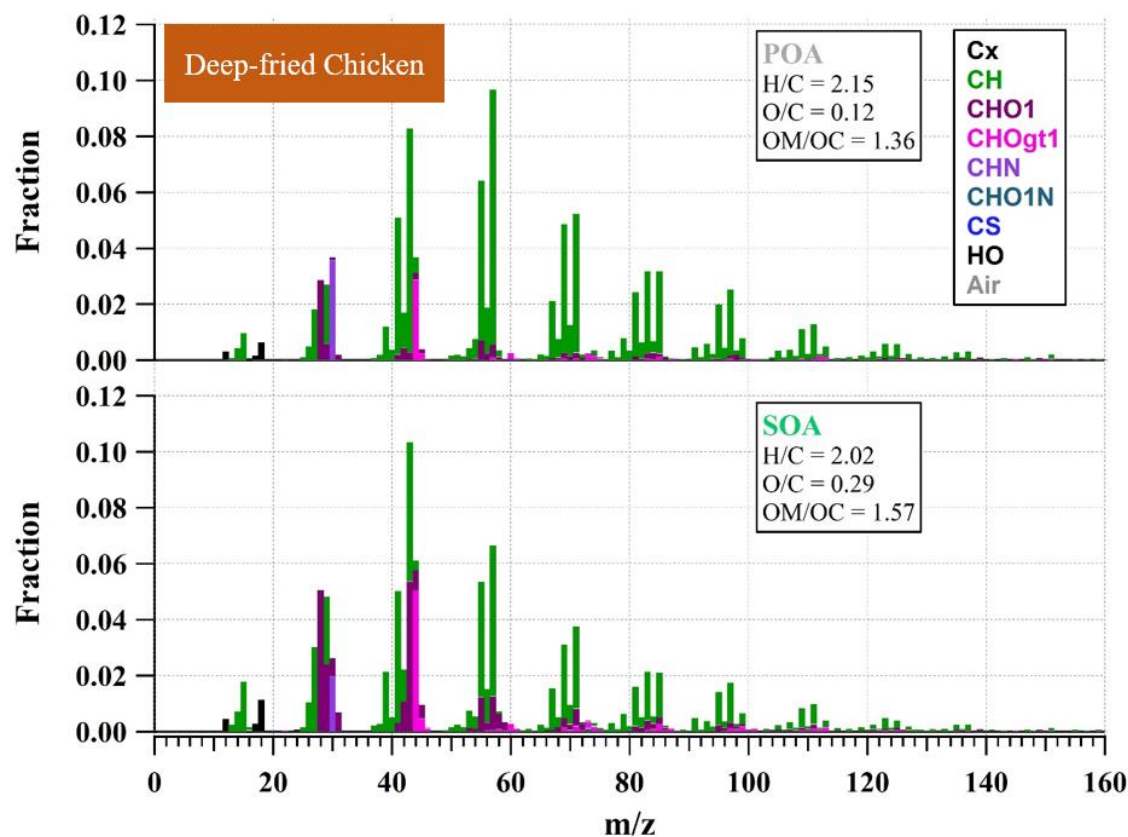


Figure S5. Mass spectra of PMF- resolved POA and SOA factors for deep-fried chicken groups.

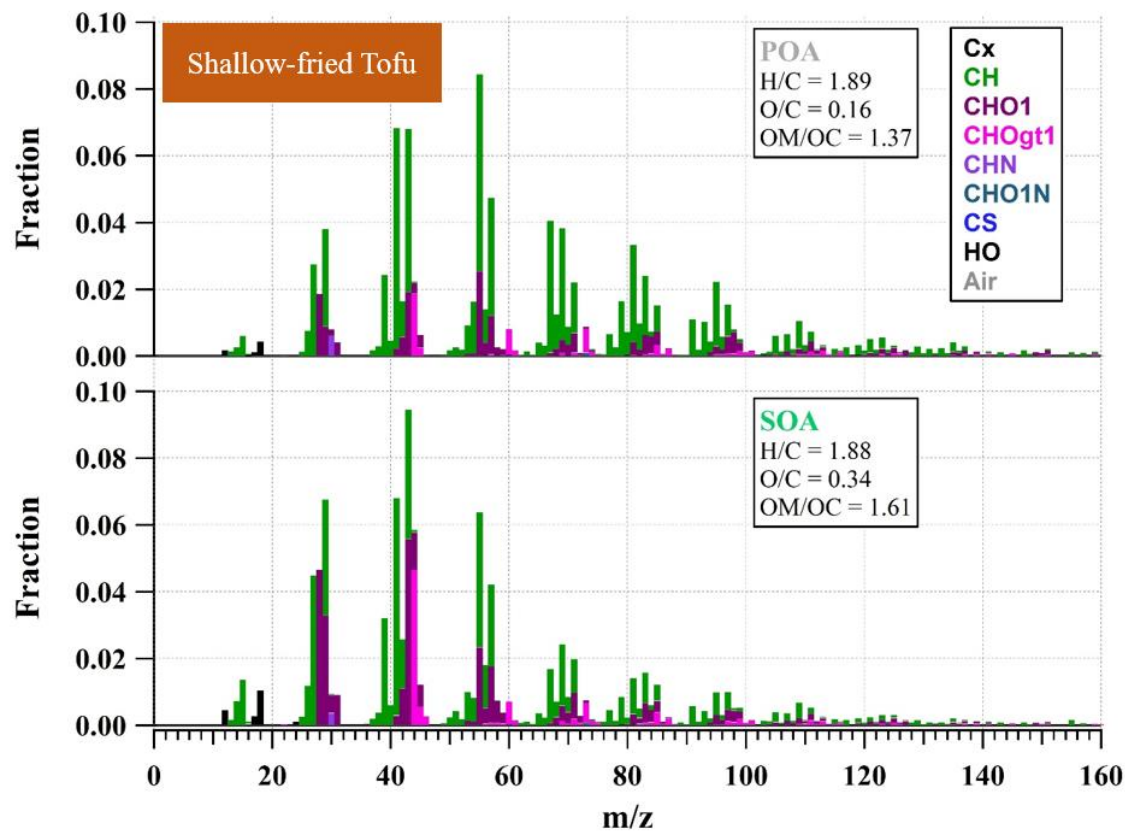


Figure S6. Mass spectra of PMF- resolved POA and SOA factors for shallow-fried tofu groups.

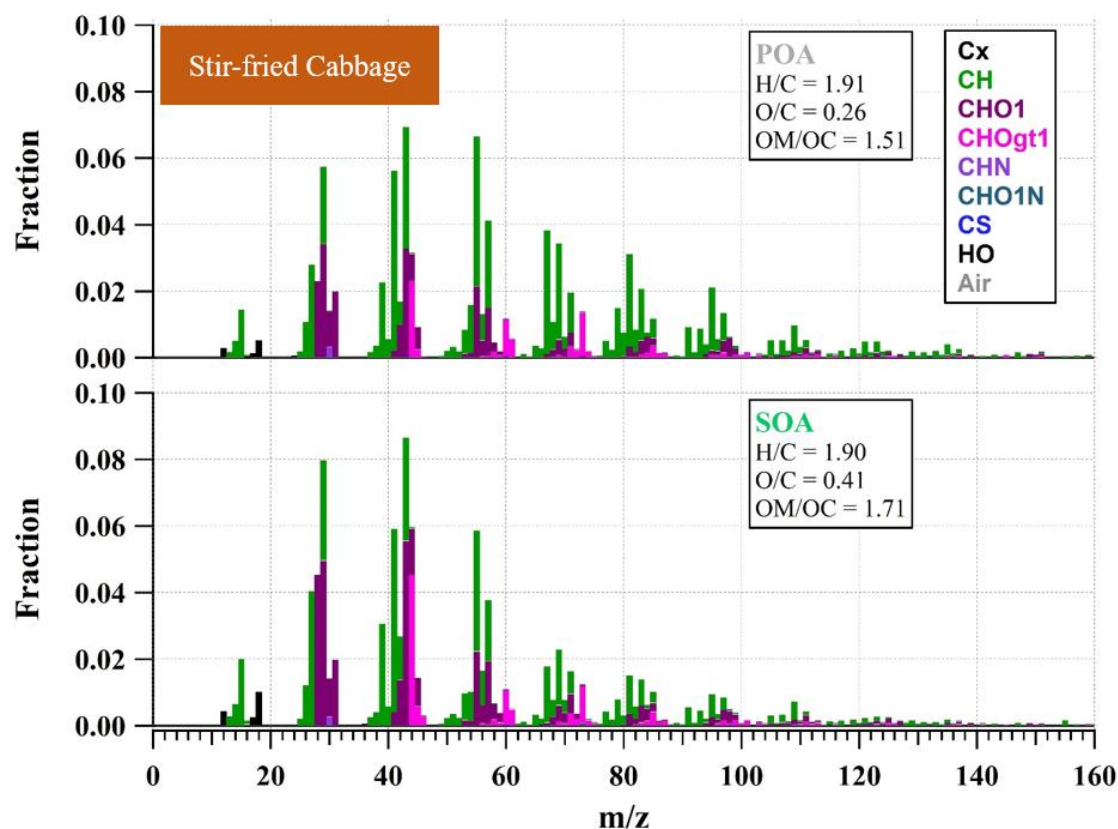


Figure S7. Mass spectra of PMF- resolved POA and SOA factors for stir-fried cabbage vegetable groups.

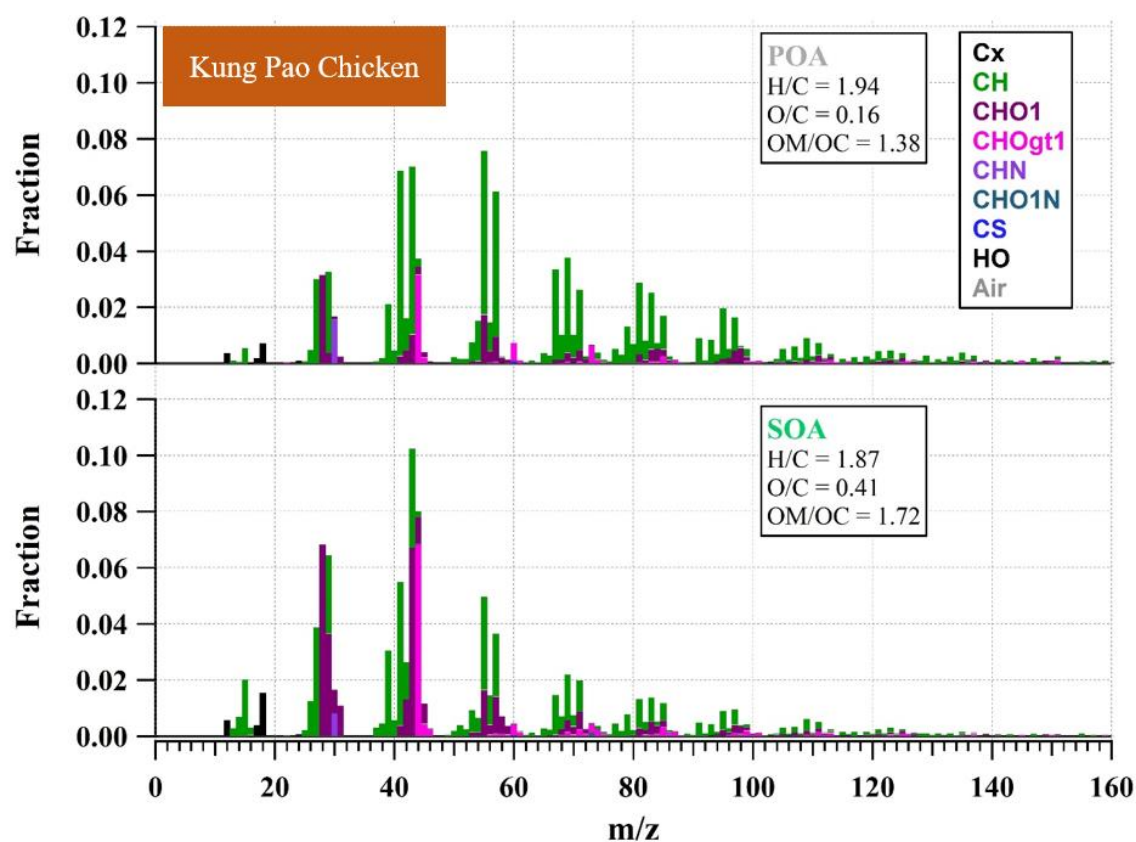


Figure S8. Mass spectra of PMF- resolved POA and SOA factors for Kung Pao chicken groups.

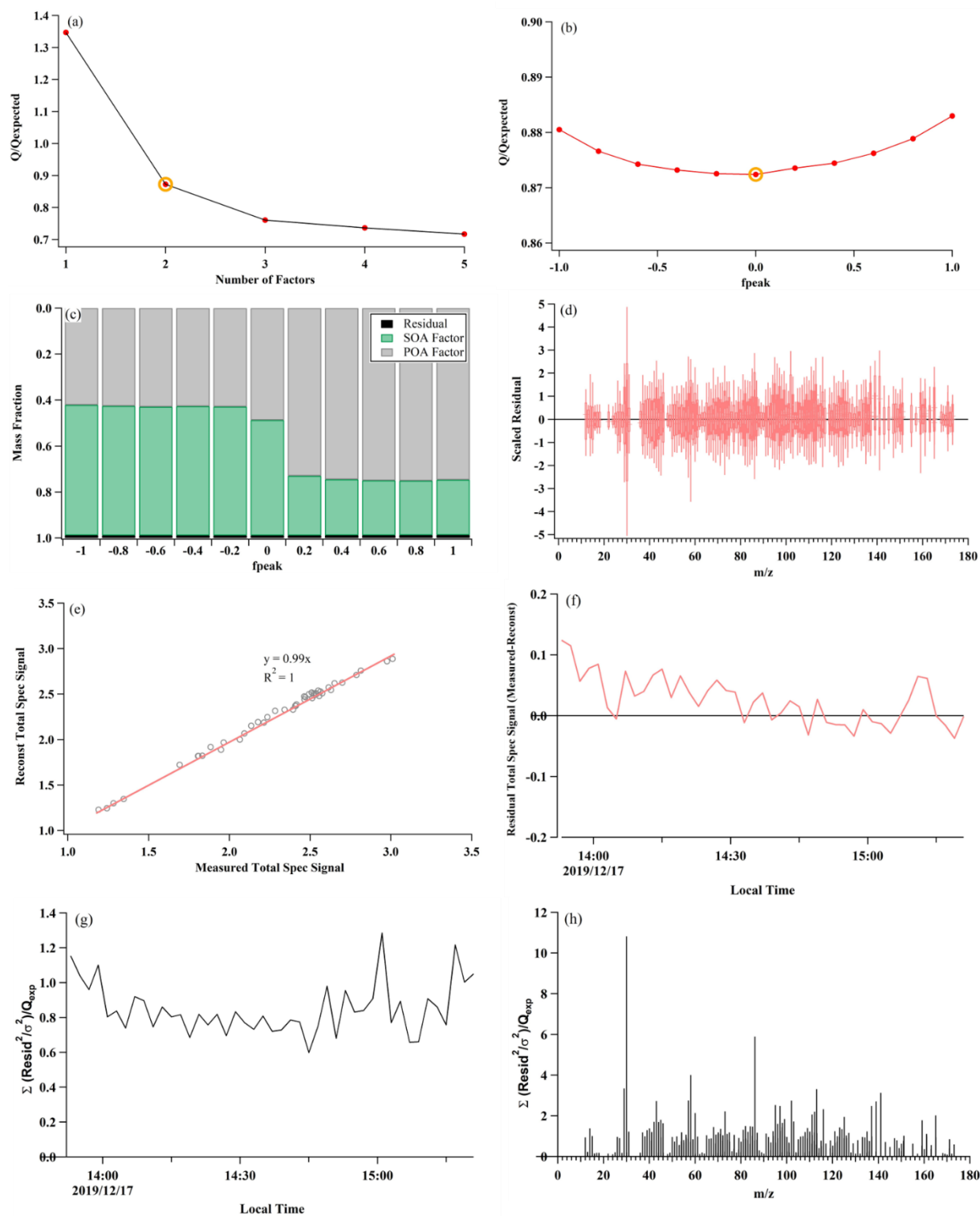


Figure S9. Diagnostic plots of the PMF analysis for deep-fried chicken groups. The following plots are shown (a) Q/Q_{exp} vs the number of factors; (b) Q/Q_{exp} vs. f_{peak} for the solution with optimal number of factors; (c) mass fraction of PMF factors vs. f_{peak} ; (d) the distribution of scaled residuals for each m/z ; (e) comparison of the reconstructed and measured total organic mass; (f) time series of the residual of PMF solutions; (g) time series of Q/Q_{exp} ; (h) the Q/Q_{exp} vs. m/z .

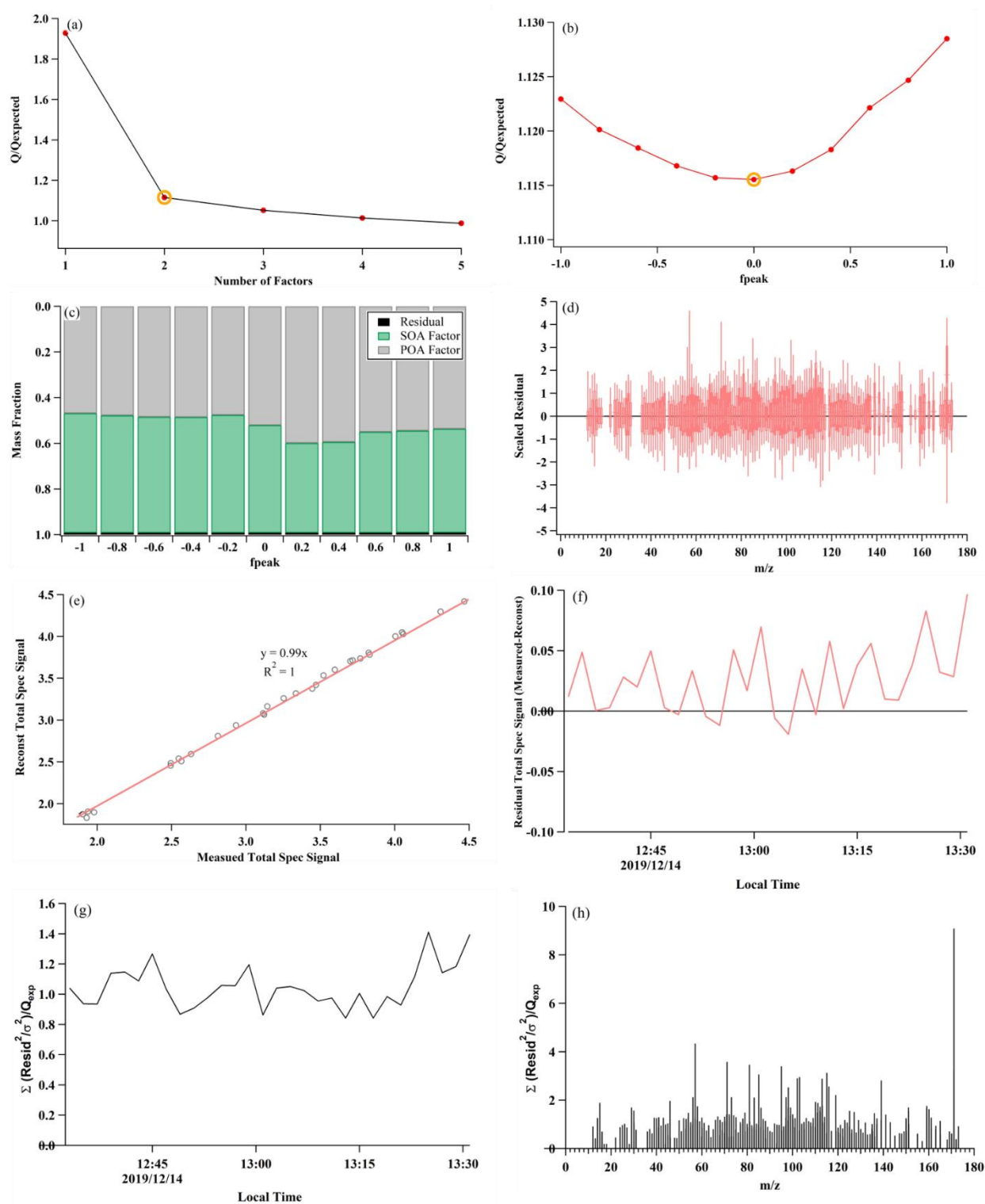


Figure S10. Diagnostic plots of the PMF analysis for shallow-fried tofu groups. The following plots are shown (a) Q/Q_{exp} vs the number of factors; (b) Q/Q_{exp} vs. f_{peak} for the solution with optimal number of factors; (c) mass fraction of PMF factors vs. f_{peak} ; (d) the distribution of scaled residuals for each m/z ; (e) comparison of the reconstructed and measured total organic mass; (f) time series of the residual of PMF solutions; (g) time series of Q/Q_{exp} ; (h) the Q/Q_{exp} vs. m/z .

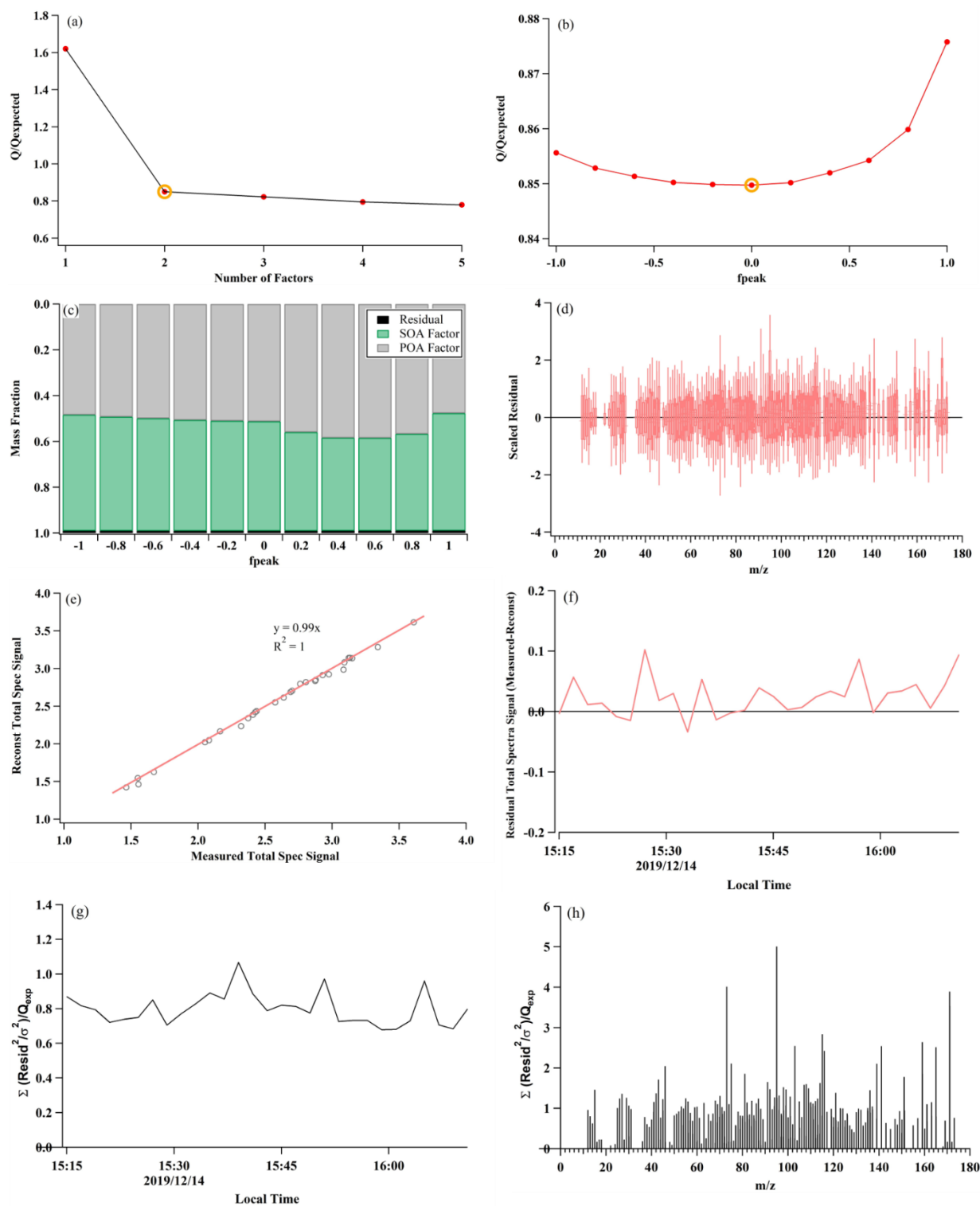


Figure S11. Diagnostic plots of the PMF analysis for stir-fried cabbage groups. The following plots are shown (a) Q/Q_{exp} vs the number of factors; (b) Q/Q_{exp} vs. f_{peak} for the solution with optimal number of factors; (c) mass fraction of PMF factors vs. f_{peak} ; (d) the distribution of scaled residuals for each m/z ; (e) comparison of the reconstructed and measured total organic mass; (f) time series of the residual of PMF solutions; (g) time series of Q/Q_{exp} ; (h) the Q/Q_{exp} vs. m/z .

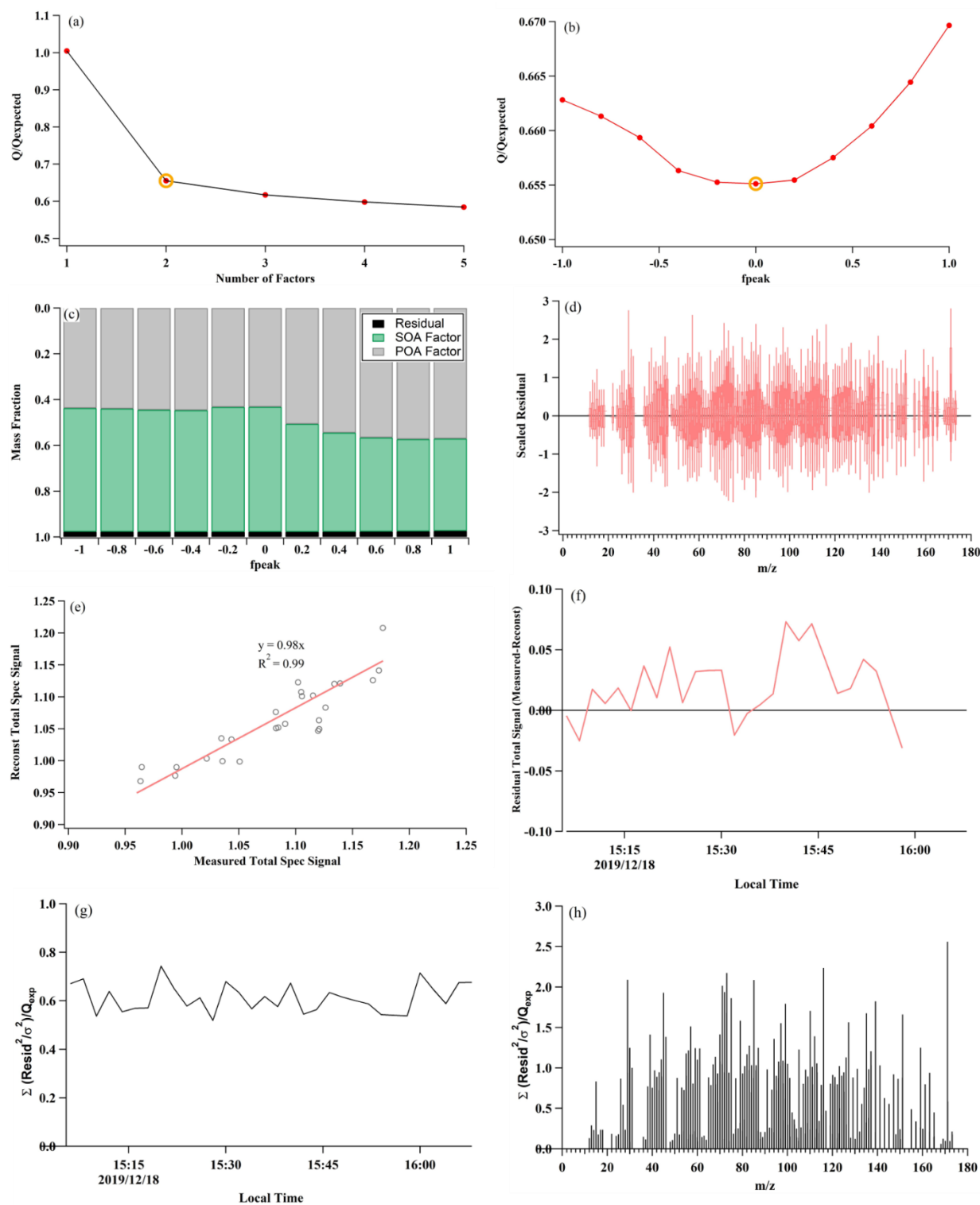


Figure S12. Diagnostic plots of the PMF analysis for Kung Pao chicken groups. The following plots are shown (a) Q/Q_{exp} vs the number of factors; (b) Q/Q_{exp} vs. f_{peak} for the solution with optimal number of factors; (c) mass fraction of PMF factors vs. f_{peak} ; (d) the distribution of scaled residuals for each m/z ; (e) comparison of the reconstructed and measured total organic mass; (f) time series of the residual of PMF solutions; (g) time series of Q/Q_{exp} ; (h) the Q/Q_{exp} vs. m/z .

References:

- Li, J., Liu, Q., Li, Y., Liu, T., Huang, D., Zheng, J., Zhu, W., Hu, M., Wu, Y., Lou, S., Hallquist, Å. M., Hallquist, M., Chan, C. K., Canonaco, F., Prévôt, A. S. H., Fung, J. C. H., Lau, A. K. H., and Yu, J. Z.: Characterization of Aerosol Aging Potentials at Suburban Sites in Northern and Southern China Utilizing a Potential Aerosol Mass (Go:PAM) Reactor and an Aerosol Mass Spectrometer, *Journal of Geophysical Research: Atmospheres*, 124, 5629-5649, 10.1029/2018jd029904, 2019.
- Li, J., Gao, W., Cao, L., Xiao, Y., Zhang, Y., Zhao, S., Liu, Z., Liu, Z., Tang, G., Ji, D., bo, H., Song, T., He, L., Hu, M., and Wang, Y.: Significant changes in autumn and winter aerosol composition and sources in Beijing from 2012 to 2018: effects of clean air actions, *Environmental pollution*, 115855, 10.1016/j.envpol.2020.115855, 2020a.
- Li, J., Liu, Z., Gao, W., Tang, G., Hu, B., Ma, Z., and Wang, Y.: Insight into the formation and evolution of secondary organic aerosol in the megacity of Beijing, China, *Atmospheric Environment*, 220, 117070, 10.1016/j.atmosenv.2019.117070, 2020b.
- Palm, B. B., Campuzano-Jost, P., Ortega, A. M., Day, D. A., Kaser, L., Jud, W., Karl, T., Hansel, A., Hunter, J. F., Cross, E. S., Kroll, J. H., Peng, Z., Brune, W. H., and Jimenez, J. L.: In situ secondary organic aerosol formation from ambient pine forest air using an oxidation flow reactor, *Atmospheric Chemistry and Physics*, 16, 2943-2970, 10.5194/acp-16-2943-2016, 2016.
- Watne, A. K., Psichoudaki, M., Ljungstrom, E., Le Breton, M., Hallquist, M., Jerksjo, M., Fallgren, H., Jutterstrom, S., and Hallquist, A. M.: Fresh and Oxidized Emissions from In-Use Transit Buses Running on Diesel, Biodiesel, and CNG, *Environmental science & technology*, 52, 7720-7728, 10.1021/acs.est.8b01394, 2018.